Assessing relative permeabilities in geothermal reservoirs using theoretical relations, laboratory measurements and field data

María Sigríður Guðjónsdóttir

School of Science and Engineering
Reykjavik University

Faculty of Industrial Engineering, Mechanical Engineering and Computer Science
University of Iceland

2015

ASSESSING RELATIVE PERMEABILITIES IN GEOTHERMAL RESERVOIRS USING THEORETICAL RELATIONS, LABORATORY MEASUREMENTS AND FIELD DATA

María Sigríður Guðjónsdóttir

120 ECTS thesis submitted in partial fulfillment of a
Philosophiae Doctor degree in Mechanical Engineering

Advisors
Guðrún Sævarsdóttir
Halldór Pálsson

Ph.D. committee
Guðrún Sævarsdóttir, Associate Professor at Reykjavik University
Halldór Pálsson, Associate Professor at University of Iceland
Guðni Axelsson, Director Geothermal Training at Iceland GeoSurvey
Jónas Elíasson, Professor Emiritus at University of Iceland

Opponents
Ronny Pini, Imperial College London
Stefan Finsterle, Lawrence Berkeley National Laboratory

School of Science and Engineering
Reykjavik University

Faculty of Industrial Eng., Mechanical Eng. and Computer Science
University of Iceland

Reykjavik, November 2015

Assessing relative permeabilities in geothermal reservoirs using theoretical relations, laboratory measurements and field data
120 ECTS thesis submitted in partial fulfillment of a PhD degree in Mechanical Engineering

School of Science and Engineering
Reykjavik University
Menntavegur 1
101, Reykjavik
Iceland
Telephone: 599 6200

Faculty of Industrial Eng., Mechanical Eng. and Computer Science
School of Engineering and Natural Sciences
University of Iceland
Sæmundargötu 2
101, Reykjavik
Iceland
Telephone: 525 4000

Bibliographic information:
María Sigríður Guðjónsdóttir, 2015, Assessing relative permeabilities in geothermal reservoirs using theoretical relations, laboratory measurements and field data, PhD thesis, School of Science and Engineering, Reykjavik University, Faculty of Industrial Eng., Mechanical Eng. and Computer Science, University of Iceland.

ISBN 978-9935-9283-5-1

Printing: Háskólaprent, Fálkagata 2, 107 Reykjavík, Iceland, November 2015

This work is dedicated to the memory of my friend, Rúnar Örn Hafsteinsson

Abstract

Liquid dominated reservoirs are a common type of hydrothermal reservoirs. They consist of fractured rock and reservoir fluid which may obey Darcy's law. Steam can form in such reservoirs either through heat input which causes temperature increase or through pressure reduction which causes flashing of the fluid. The modified Darcy's law for two phase reservoirs uses relative permeabilities to account for the area reduction of the phases. Darcy's law was used in this thesis to calculate the relative permeabilities for a fluid which flashes in a hydrothermal reservoir and a comparison was made for two flow cases, horizontal and vertical flow. The results show that there is a significant difference in the relative permeabilities between the two flow cases although they share identical transport and thermodynamic properties. This effect of gravity on the relative permeabilities was also observed when measurements were made using water and air as the two phases. Laboratory measurements were also performed to calculate the relative permeabilities of water and steam of geothermal origin. The resulting relative permeabilities showed a tendency to follow the Corey curve to some extent. The so called Shinohara method was used on data from two phase geothermal wells to calculate the relative permeabilities in the reservoirs. The reservoirs consist of a fractured medium rather than porous and the relative permeabilities there show less interaction than in the experiments. The results are an important contribution to understanding the behaviour of two phase flow through a geothermal reservoir. They can be used for geothermal modelling, thus contributing to more detailed modelling of geothermal reservoirs.

Útdráttur

Votgufusvæði sem eru algeng tegund jarðhitasvæða samanstanda af sprungnu bergi og jarðhitavökva sem flæðir m.a. samkvæmt Darcy lögmálinu. Gufa getur myndast í slíku jarðhitakerfi við varmainnstreymi sem veldur hitastigshækkun eða með þrýstingslækkun vökvans sem veldur hvellsuðu. Darcy jöfnur fyrir tveggja fasa flæði innihalda hlutlektir sem taka mettun fasanna með í reikninginn. Í þessari ritgerð var Darcy lögmálið notað til að reikna hlutlektir vökva sem hvellsýður í jarðhitakerfi og samanburður var gerður á tveimur flæðistilfellum, láréttu og lóðréttu. Niðurstöðurnar sýna að munur er á hlutlektunum í þessum tilfellum þrátt fyrir að eiginleikar þeirra séu að öðru leyti þeir sömu. Þessi áhrif þyngdarafls á hlutlektirnar sáust einnig þegar mælingar voru gerðar á vatni og lofti. Tilraunir voru einnig gerðar þar sem mældar stærðir voru notaðar til að reikna hlutlektir vatns og gufu úr jarðhitavökva. Hlutlektirnar fylgdu Corey ferlunum að nokkru leyti. Svokölluð Shinohara aðferð var notuð á gögn frá borholum jarðhitasvæða til að reikna hlutlektir í tveggja fasa jarðhitakerfunum. Jarðhitakerfin samanstanda frekar af sprungnu frekar en gljúpu bergi og hlutlektirnar benda því til minni víxlverkana milli fasanna heldur en tilraunirnar sýndu. Niðurstöðurnar auka skilning á hegðun vatns og gufu í jarðhitakerfum og stuðla þær að bættum reiknilíkönum fyrir jarðhitakerfi.

List of publications

This dissertation is based on the following original submitted and published papers, which are referred to in the text by their Roman numbers (I-IV)

I. **The effect of gravity on the application of relative permeabilities in modelling two phase geothermal reservoirs**
Maria Gudjonsdottir, Halldor Palsson, Jonas Eliasson, Gudni Axelsson, Gudrun Saevarsdottir
Submitted to Water Resources Research.

II. **Water and air relative permeabilities from laboratory experiments. The effect of gravity on Darcy's law**
Maria Gudjonsdottir, Halldor Palsson, Jonas Eliasson, Gudrun Saevarsdottir
Submitted to Water Resources Research.

III. **Calculations of relative permeabilities of water and steam from laboratory measurements**
Maria Gudjonsdottir, Halldor Palsson, Jonas Eliasson, Gudrun Saevarsdottir
Geothermics, Vol. 53, pp. 396-405 (2015).

IV. **Calculations of relative permeabilities from field data and comparison to laboratory measurements**
Maria Gudjonsdottir, Halldor Palsson, Jonas Eliasson, Gudrun Saevarsdottir
Geothermics, Vol. 54, pp. 1-9 (2015).

The papers and the manuscripts do not appear in the on-line version of this thesis.

Conference publications that have been written and presented about the content of the dissertation consist of:

A. **Relative permeability measurements and comparison to field data**
Maria Gudjonsdottir, Halldor Palsson, Jonas Eliasson, Gudrun Saevarsdottir
Proceedings World Geothermal Congress 2015, Melbourne, Australia, 19-25 April 2015.

B. **Measurements of relative permeabilities of water and steam**
Maria Gudjonsdottir, Jonas Eliasson, Halldor Palsson, Gudrun Saevarsdottir
Proceedings, Thirty-Eighth Workshop on Geothermal Reservoir Engineering, Stanford University, Stanford, California, February 11-13, 2013.

C. **Effect of flow configuration on the relative permeabilities of water and steam in two phase flow in geothermal reservoirs**
Maria Gudjonsdottir, Jonas Eliasson, Gudni Axelsson, Halldor Palsson, Gudrun Saevarsdottir
Proceedings, Thirty-Seventh Workshop on Geothermal Reservoir Engineering, Stanford University, Stanford, California, January 30-February 1, 2012.

D. **Assessing relative permeabilities of two phase flows of water and steam in geothermal reservoirs: State of the art relations**
Maria Gudjonsdottir, Jonas Eliasson, William Harvey, Halldor Palsson, Gudrun Saevarsdottir. GRC Transactions, Vol. 34, 2010.

Declaration of contribution

Paper I - María Sigríður Guðjónsdóttir made the calculations, wrote the manuscript and corresponds with the journal.

Paper II - María Sigríður Guðjónsdóttir supervised the initial design and installation of the measurement device and made improvements, conducted the experiments, processed and analysed the results, wrote the manuscript and corresponds with the journal.

Paper III - María Sigríður Guðjónsdóttir designed and installed the measurement device, conducted the experiments, processed and analysed the results, wrote the manuscript and corresponded with the journal.

Paper IV - María Sigríður Guðjónsdóttir collected the data for the calculations, performed the calculations, analysed the results, wrote the manuscript and corresponded with the journal.

Contents

List of Figures

List of Tables

Nomenclature

A	Cross sectional area	[m^2]
b	Fracture aperture	[m]
D	Section 3.1.2: Depth	[km]
D	Diameter	[m]
d_e	Effective grain size	[m]
f_g	Force due to gravity	[N/m^3]
f_ν	Viscous force	[N/m^3]
g	Gravitational acceleration	[m/s^2]
h	Enthalpy	[kJ/kg]
k	Intrinsic permeability	[m^2]
k_r	Relative permeability	[−]
ΔL	Length of a flow channel	[m]
L	Section 2.1: Characteristic length scale	[m]
L	Section 2.2 Length of a flow channel	[m]
L	Section 3.1: Height of a convection cell	[m]
$\dot{m}$	Mass flow	[kg/s]
n	Section 2.1: Unit normal	[−]
p	Pressure	[Pa] or [bar]
$\frac{\Delta p}{\Delta x}$	Pressure gradient	[Pa/m]
p_c	Capillary pressure	[Pa]
q	Mass flux	[kg/m^2s]
Q^*	Parameter for the Shinohara method	[kg/s]
Re	Reynolds number	[−]
S_r	Residual saturation	[−]
S_w	Water saturation	[−]
$S_{w,f}$	Flowing water saturation	[−]
S_{wn}	Normalized water saturation	[−]
t	Thickness	[m]
T	Temperature	[℃]
V	Volume	[m^3]
$\dot{V}$	Volumetric flow rate	[m^3/s]
v	Section 2.1: Local flow velocity	[m/s]
v	Section 2.2: Specific volume	[m^3/kg]
x	Mass fraction	[−]

Greek symbols

α	Contact angle	[−]
β	Non-Darcy coefficient	[1/m]
λ	Pore size distribution index	[−]
μ	Dynamic viscosity	[kg/(ms)]
μ_r	Viscosity ratio	[−]
ν	Kinematic viscosity	[m^2/s]
ρ	Density	[kg/m^3]
σ	Surface tension	[N/m]

Subscripts

a	Air
α	Phase notation
β	Phase notation
end	End condition
f	Flowing
hor	Horizontal
i	Inlet condition
in	Initial condition
o	Outlet condition
s	Steam
t	Total
ver	Vertical
w	Water

Acknowledgments

Many people contributed to this work in one way or another. All the people involved in the designing and building the laboratory equipment contributed greatly, which I thank them for, although all their names are not listed her. The laboratory equipments used for this research was installed at several locations. I would like to thank the companies and institutions who housed the experiments. They were: Reykjavik University, Keilir Atlantic Center of Excellence, Innovation Center Iceland (NMÍ) and HS Orka. I would especially like to thank all the kind people at the laboratories and power plant where the laboratory equipments were installed and operated. Óðinn Bolli Björgvinsson at Keilir, Eiríkur Þorsteinsson at NMÍ, the operators at Reykjanes power plant and Gísli Freyr Þorsteinsson at Reykjavik University. I am also very grateful to Vilhjálmur Sigurjónsson at University of Iceland and Hörður Steingrímsson at Framtak for their assistance. Operating the laboratory equipment was not always a single person task, and I would like to thank the graduate students who assisted me with the experients: Jón Rafn Valdimarsson, Baldur Kárason, Carlos Cordova and Vijay Chauhan. Also I would like to thank Samuel Perkins for all the English proofreading.

I would like to thank the power companies, Reykjavik Energy and HS Orka who provided data for my research and Reykjavik Energy for providing piping material for the experimental device. Special thanks to Gunnar Gunnarsson, Andri Arnaldsson, Geir Þórólfsson, Daði Þorbjörnsson, Þráinn Friðriksson, Malcolm Grant and Roland Horne for their advice.

Financing this project was an important factor for paying salaries and buying laboratory equipment. Following companies, funds and institutions supported this project: Landsvirkjun Energy Fund, Orkusjóður (contract no. 30-2013), Geothermal Research Group (GEORG, project ID 09-01-011), Íslandsbanki study grant and University of Iceland Equipment Fund. Geothermal Association of Iceland, University of Iceland and GEORG granted travel grants. All this support is highly appreciated.

I would especially like to thank my advisors, Guðrún Sævarsdóttir and Halldór Pálsson for their contribution. They inspired me throughout this research and gave valuable advice. I also would like to thank other members of the doctoral committee, Jónas Elíasson and Guðni Axelsson for their contribution and inspiration in research

of geothermal reservoirs.

Going through a Ph.D. study includes good and bad days. I would like to thank my fellow Ph.D. students and staff at RU for all the lunch and coffee breaks which could easily change a bad day into a good one. I would also like to thank my friends and family for the moral support throughout the project time.

Last but not least, thank you Nökkvi, Pálmi, Huldar and Dagur for existing and being the most important part of my life.

1 Introduction

1.1 General description

Using geothermal energy for power production and direct utilization is considered to be a more environmentally friendly energy option than using conventional energy sources like fossil fuels or nuclear energy. In 2015 the global installed capacity of electrical power using geothermal energy sources is around 12.6 GW_e (Bertani, 2015) and over 70 GW_{th} for direct utilization (Lund and Boyd, 2015). This study pertains to high temperature hydrothermal reservoirs which are the geothermal resource type mainly utilized to date.

Geothermal resources must first be explored and analysed before they can be utilized for energy production, and must be carefully monitored once in operation to ensure that the resource is used in a sustainable way. One of the tools used for reservoir monitoring and forecasting is reservoir modelling. Reservoir modelling involves computer simulation of the reservoir characteristics and its behaviour prior to, during and after utilization periods. The use of models includes the calculation of coupled mass and energy balance of the reservoir components during a predefined time. Through geothermal reservoir modelling, the future fluid flow from the wells is estimated (Grant, 1983). Certain parameters need to be known or estimated prior to the modelling, like reservoir properties (permeability and porosity) and thermodynamic properties depending on the phenomena that are being modelled. Inverse modelling can be applied where the field history of testing and exploitation of geothermal fields are used to determine the reservoir properties (Finsterle et al., 1997). Forward and inverse modelling can then be applied to predict the reservoir behaviour in detail.

In this context it is useful to review the definitions of a geothermal resource and reserve, geothermal field, geothermal system and geothermal reservoir as demonstrated in Fig. 1.1. A geothermal field is an area where a geothermal reservoir can be found below. The geothermal system includes recharge water streams and the reservoir as well as the flow out of the system. The geothermal reservoir is the part of the geothermal system which has high temperature fluid and is permeable and can therefore be exploited for thermal energy or electricity production. Finally,

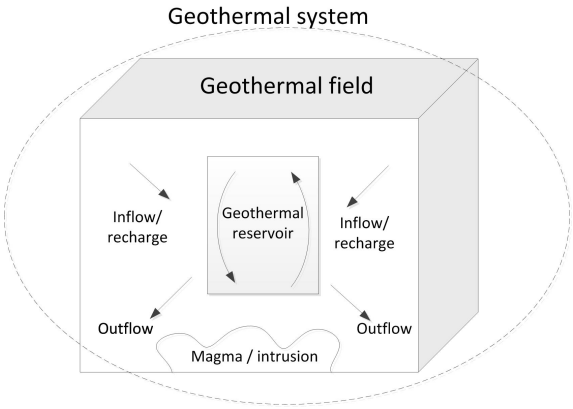

Figure 1.1: Representation of a geothermal field, a geothermal system and a geothermal reservoir.

geothermal resources or geothermal reserves refer to the energy content that the reservoir possesses for utilization. The heat source is generally a magma intrusion at few kilometres depth below the reservoir.

Geothermal reservoirs are classified into low, medium or high temperature/enthalpy reservoirs depending on their temperature (Axelsson, 2008), (Bodvarsson, 1961), (Axelsson and Gunnlaugsson, 2000). Low temperature reservoirs are defined where reservoir temperature at 1 km depth is below 150℃ and high temperature reservoirs are defined where the temperature at 1 km depth is above 200℃, but these temperature ranges can be subdivided more specifically (Sanyal, 2005). The reservoirs are also divided into steam dominated, two-phase or liquid dominated reservoirs with regard to the dominating phase of the geothermal fluid.

In general, for the common type of liquid dominated reservoirs, the geothermal fluid exists either as single phase water or a mixture of water and steam where the water is still the dominating phase. The geothermal fluid contains dissolved gasses and solids (Arnorsson et al., 2007), but is often considered to be pure water or steam when its flow through the permeable matrix is modelled and simulated. Phase changes and the presence of chemical species have however been adopted in many numerical simulations (O'Sullivan et al., 2001).

The two phase mixture of water and steam in liquid dominated reservoirs can form under different conditions. Boiling can occur due to pressure reduction of the fluid and a two phase mixture is formed at saturated conditions. Such a system as suggested by White (1967) is described as a conceptual model in Fig. 1.2a. In the figure the heat source is assumed to be a magma intrusion at a depth of a few kilometres, conducting heat through an impermeable layer to the porous and fractured matrix above which is defined as the reservoir. The groundwater fluid filtrates through the permeable layers into the reservoir, where its enthalpy increases due to the con-

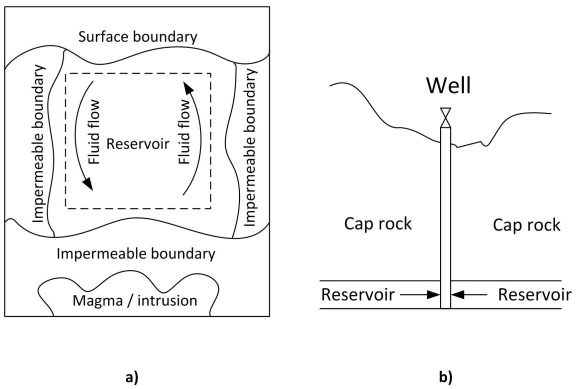

Figure 1.2: a) Convective system representing a convective volcanic geothermal reservoir b) A figure showing where a geothermal well is drilled into a reservoir, causing fluid to flow through the fractured reservoir into the well.

ducted heat from the heat source. Consequently, the fluids temperature increases, and its density decreases, causing it to flow upwards due to buoyancy effects. The pressure of the fluid also decreases as it flows through the resistive matrix in the reservoir. This may cause the fluid to reach saturation pressure at which it undergoes flash boiling, forming steam, which results in a two phase fluid. At the upper boundary of the reservoir the fluid becomes colder than the fluid below and flows down again. The arrows in Fig. 1.2a refer to the fluid flow in the reservoir.

Another mechanism resulting in two phase flow in a liquid dominated reservoir is where production wells have been drilled into the reservoir to extract fluid for utilization. When the fluid is extracted through the wells, flashing can occur due to pressure drop near the well. The high enthalpy fluid reaches saturation through the pressure reduction and steam begins to form. The flash horizon (the point where flashing starts) may exist in the well or in the porous surroundings where the fluid is approaching the well (DiPippo, 2008) thus creating two phase fluid in the reservoir. In geothermal reservoirs, fluid mainly flows to the well through few fissures (Grant and Bixley, 2011) but this flow is often simulated using Darcy's law (Chen et al., 2004), (Chen and Horne, 2006) which has been shown to be valid for fracture flow (Chen, 2005). A schematic showing the geothermal reservoir and the well is shown in Fig. 1.2b.

Darcy's law can be used to model the flow of a fluid through a porous matrix such as in oil and gas reservoirs, geothermal reservoirs and other situations involving groundwater flow. For a two phase flow, the concept of relative permeabilities has been introduced in order to account for the phase area reduction. An empirical adaptation of Darcy's law for two phase flow was presented by Wyckoff and Botset (1936) and is believed to be the first publication defining relative permeability curves based on experiments (Chen, 2005). Certain challenges arise when applying Darcy's law for two phase flow in geothermal reservoirs as will be introduced in Section 1.2

where the motivation and objectives for this study is described.

1.2 Motivation, objectives and goals

The relative permeabilities are important parameters in geothermal reservoir modelling since they determine the steam and water amount in the reservoir flow and are also used to determine properties like total viscosity and flowing enthalpy of the two phase mixture. When modelling two phase flow of fluid through a geothermal reservoir, Darcy's law is normally used in a modified form. These resulting equations contain the relative permeabilities and the relative permeability curves need to be arbitrarily selected before modelling takes place. Several uncertainties have to be dealt with when using relative permeabilities in geothermal modelling. A better determination of these parameters can prevent overestimation of the reservoir performance and can contribute to improved utilization of geothermal reservoirs. It is important to study the effect that the geothermal fluid has when applying Darcy's law. It is also important to study the effect of flow direction on the relative permeabilities. To meet this need the following objectives were defined:

- To analyse the effect of gravity on the relative permeabilities in two phase flow in a porous medium by using state of the art relations
- To perform measurements on two phase flow in porous medium to observe its behaviour with respect to gravity
- To design and construct an experimental device that can mimic reservoir properties up to certain extents
- To conduct experiments of two phase flow through porous media with parameter variations
- To compare the relative permeabilities obtained in experiments to field data

By performing the project tasks, the following goals were under consideration:

- To analyse the behaviour of two phase flow and its relative permeabilities with respect to gravity
- To assess the relative permeabilities of two phase flow through a porous medium using real geothermal fluid
- To estimate the applicability of the relative permeability curves when modelling geothermal reservoir by using calculated values of relative permeabilities from field data

In the next Chapter 2 the theoretical background for this thesis as well as literature review is presented.

2 Background

2.1 Darcy's law

2.1.1 Single phase flow

Henry Darcy, a French hydrologist, reported a relation for groundwater flow for the city of Dijon (Darcy, 1856). His empirically stated equation can also be analytically derived from the Stokes equations (Whitaker, 1986). Darcy's law is shown in Eq. (2.1) and relates the mass flux $\vec{q}$ for a single phase, incompressible fluid with kinematic viscosity ν and density ρ flowing through a permeable matrix with intrinsic permeability k to the pressure gradient ∇p and the hydrostatic pressure $\rho\vec{g}$ which acts on the fluid.

$$\vec{q} = -\frac{k}{\nu}(\nabla p - \rho\vec{g}) \tag{2.1}$$

The applicability of Darcy's law is determined by the Reynolds number which is defined in Eq. (2.2).

$$Re = \frac{vL}{\nu} \tag{2.2}$$

where v is the local velocity of the fluid and L is the characteristic length scale. Darcy's law in Eq. (2.1) is valid for relatively low Reynolds numbers. When determining the number for flow in porous media the characteristic length used in Eq. (2.2), L, becomes the effective grain size d_e. Various determinations of the effective grain size are found in the literature, usually they range between 10% (Todd and Mays, 2005) and 30% of the passing sieve diameter. Darcy's law is applicable for the Reynolds number, Re < 1, and this limit has in some cases been extended up to 10 or higher (Zeng and Grigg, 2006). Thus, the limit is not general, and for a given flow case, a linearity between the mass flux and the pressure gradient has to be assured for Eq. (2.1) to be valid.

If inertia effects become significant for the fluid flow, another term accounting for the non-Darcy behaviour of the flow in the porous medium has to be added leading to the Darcy-Forchheimer (Forchheimer, 1901), (Ahmed and Sunada, 1969) equation showing the pressure gradient in Eq. (2.3).

$$-\nabla p = \frac{\mu v}{k} + \beta \rho v^2 \tag{2.3}$$

where β is the non-Darcy coefficient and μ is the dynamic viscosity of the fluid.

2.1.2 Two phase flow

When Eq. (2.1) is applied on multiphase flow such as two phase flow in geothermal reservoirs, that equation alone is not sufficient. Therefore the concept of relative permeabilities has been introduced. It was first introduced by Buckingham in 1907 (Ambusso 1996) and has been widely used in oil and gas reservoir studies and other studies regarding multiphase flow since then. The relative permeability, k_r, acts as a permeability reduction factor for the individual phase permeability. For flow of two phases characterized with α and β Eq. (2.1) becomes Eqs (2.4) and (2.5).

$$\vec{q_\alpha} = -\frac{k k_{r\alpha}}{\nu_\alpha}(\nabla p_\alpha - \rho_\alpha \vec{g}) \tag{2.4}$$

$$\vec{q_\beta} = -\frac{k k_{r\beta}}{\nu_\beta}(\nabla p_\beta - \rho_\beta \vec{g}) \tag{2.5}$$

where the subscripts α and β represent the two phases. In geothermal reservoirs, the phases are the vapour and the liquid form of the same substance, water. Grant and Bixley (2011) reported Eqs (2.4) and (2.5) using the same pressure gradient for both phases leading to Eqs (2.6) and (2.7) for water and steam.

$$\vec{q_w} = -\frac{k k_{rw}}{\nu_w}(\nabla p - \rho_w \vec{g}) \tag{2.6}$$

$$\vec{q_s} = -\frac{k k_{rs}}{\nu_s}(\nabla p - \rho_s \vec{g}) \tag{2.7}$$

where the subscripts w and s represent water and steam respectively. Whether the same pressure gradient can be applied to both phases depends on the magnitude of

the capillary pressure in the two phase flow. The effect of capillary pressure is small and often ignored in geothermal reservoir engineering (Weir, 1991), (Li and Horne, 2007), Li and Horne (2005b) The capillary pressure p_c in a mixture of water and steam is defined as shown in the following Eq. (2.8).

$$p_c = p_s - p_w \tag{2.8}$$

where p_s and p_w are the steam and water pressure respectively. The definition of the capillary pressure between two phases in a parallel-plate fracture is as shown in Eq. (2.9)

$$p_c = \frac{2\sigma \cos \alpha}{b} \tag{2.9}$$

where σ is the surface tension for the wetting phase (in this study, liquid water), α is the contact or wetting angle for the water-steam surface on the three phase junction with the solid and b is the aperture of the fracture (Pruess and Tsang, 1990).

Various models have been reported for determining capillary pressure in porous and fractured media (Brooks and Corey, 1964), (Li and Horne, 2006). In their work, Li and Horne (2004) showed that the steam-water capillary pressure can be significantly lower than for air-water mixture. Li and Horne (2007) proposed two different models for the determination of capillary pressure in geothermal systems, one for drainage case (where water is gradually replaced by steam over the saturation range) and other for the imbibition case (where steam is gradually replaced by water over the saturation range). According to these relations, imbibition capillary pressure is usually lower than for the drainage case.

It should always be considered whether the capillary pressure should be accounted for in the thermodynamic properties of the steam phase when using Eqs (2.4) and (2.5) prior to modelling of the two phase flow. Also it should be considered if the pressure gradient can be assumed to be the same for the water and the steam phase, that is if Eqs (2.6) and (2.7) can be used instead of Eqs (2.4) and (2.5). In his study, Piquemal (1994) measured the capillary pressure and found it to be constant through the core used for the experiments and therefore the same pressure gradient could be used for both phases and in the literature it varies between studies whether the capillary pressure is taken into account or not.

When the relative permeabilities are estimated for reservoir flow or laboratory experiments, it can be more convenient to use the mass flow definition by applying

Eq. (2.10) instead of the mass flux in Eq. (2.1).

$$\dot{m} = A\vec{n} \cdot \vec{q} \tag{2.10}$$

where $\vec{n}$ is the unit normal to the cross sectional area A of the porous flow channel. That gives us Eqs (2.11) and (2.12) from Eqs (2.6) and (2.7) to determine the mass flow of the water and the steam respectively by using the relative permeabilities k_{rw} and k_{rs}.

$$\dot{m}_w = -\frac{kk_{rw}}{\nu_w} A\vec{n} \cdot (\nabla p - \rho_w \vec{g}) \tag{2.11}$$

$$\dot{m}_s = -\frac{kk_{rs}}{\nu_s} A\vec{n} \cdot (\nabla p - \rho_s \vec{g}) \tag{2.12}$$

Scheidegger (1974) presented a relation which takes the compressibility of the gaseous phase into account, shown in Eq. (2.13) for a one dimensional flow of steam perpendicular to gravity.

$$q_s = -\frac{kk_{rs}(p_i^2 - p_o^2)}{2p_o \Delta L \nu_s} \tag{2.13}$$

where p_i and p_o are the inlet and outlet pressures in a permeable section of a flow channel of length ΔL. When two phases are flowing simultaneously, the flowing mass fraction of the gaseous phase can be determined by the mass flows of the two phases according to Eq. (2.14)

$$x = \frac{\dot{m}_s}{\dot{m}_s + \dot{m}_w} \tag{2.14}$$

where the $\dot{m}_w$ and $\dot{m}_s$ are the mass flows of water and steam respectively. The mass flow of each phase can then be determined from Eqs (2.15) and (2.16).

$$\dot{m}_w = (1 - x)\dot{m}_t \tag{2.15}$$

$$\dot{m}_s = x\dot{m}_t \tag{2.16}$$

where $\dot{m}_t$ is the total mass flow of water and steam. For reservoir fluid with known total specific enthalpy in the flow, h_t, the steam fraction of the fluid, x, can be defined from Eq. (2.17).

$$x = \frac{h_t - h_w}{h_s - h_w} \tag{2.17}$$

where h_w and h_s are the saturation enthalpies for water and steam respectively.

Water saturation is an important parameter in water and steam flow in a permeable material and can be used to determine the relative permeabilities. The water saturation of the two phase mixture is defined in Eq. (2.18).

$$S_w = \frac{V_w}{V_w + V_s} \tag{2.18}$$

where V_w and V_s are the volumes of water and steam respectively in a control volume. For a one dimensional flow, the water saturation can be defined with Eq. (2.19).

$$S_w = \frac{A_w}{A_w + A_s} \tag{2.19}$$

where A_w and A_s are the cross sectional areas occupied by the water and steam respectively in the total cross sectional area of the flow channel.

2.2 Relative permeabilities

2.2.1 Determination of relative permeabilities

The relative permeabilities used in Eqs (2.11) and (2.12) account for the permeability reduction in the modified Darcy's law that treat the phases separately in the two phase mixture flow. The relative permeabilities tell us the phases ability to flow with regard to the presence of the other. The relative permeabilities are normally presented as functions of the wetted saturation, S_w, defined in Eq. (2.18) or Eq. (2.19). If the relative permeabilities would only account for the area ratio occupied by each phase the relative permeabilities would follow the water saturation, S_w linearly and follow the so called X-curves.

Many studies have been performed on relative permeabilities of two phase flows using different substances both in fractured and porous media. A number of those studies have included air-water or nitrogen-water flow as well as water and steam. The studies have resulted in different findings regarding whether phase transformation has an effect on the relative permeabilities or not. When results of steam and water flow are compared to nitrogen-water flow or air-water flow using the same experimental setup, the relative permeabilities for the steam phase seem to be higher than for the nonwetting phase (the gaseous phase) for the air-water and nitrogen-water experiments (Chen, 2005) (Chen et al., 2007). That indicates that the boiling mechanism induces the flow of the steam where in absence of boiling the two phases seem to restrain the flow of each other to a greater extent.

Various experiments have been made in the past in order to calculate the relative permeabilities of water and steam flow in porous or fractured media. These studies show, that the X-curves can hardly be expected to sufficiently describe the relative permeabilities of water and steam. Table 2.1 summarizes previous experiments made in this field and Fig. 2.1 shows the resulting relative permeabilities as function of the water saturation. They are plotted together with the Corey curves and the X-curves where the residual saturations are $S_{wr} = 0.25$ and $S_{sr} = 0.05$. The residual saturations define the mobile region of the two phases. In Fig. 2.2 these experimental results of the relative permeabilities for water and for steam are plotted against each other. As seen from Figs 2.1 and 2.2 no fundamental set of curves describing the relative permeabilities has been developed for water and steam in particular.

Table 2.1: Experiments found in the literature for determining relative permeabilities of water and steam, D = inner diameter of flow channel, L = length of flow channel, k = intrinsic permeability (1 Darcy = 10^{-12} m^2).

Reference	Filling	Dimensions
(Ambusso, 1996), (Mahiya, 1999), (Satik, 1998), (O'Connor, 2001)	Berea sandstone core k = 0.6 Darcy	D = 5.08 cm L = 43.2 cm
(Piquemal, 1994)	Unconsolidated quartz sand k = 3.78-3.96 Darcy	D = 5 cm L = 25 cm
(Verma, 1986)	Glass beads k = 0.64 Darcy	D = 7.62 cm L = 100 cm
(Sanchez et al., 1986) (Sanchez and Schechter, 1990)	Silica sand k = 7.3 Darcy	D = 3.18 cm L = 19.5 cm

Different methods have been used to determine the water saturation in flow channels during laboratory experiments of relative permeabilities. A possible method is to use X-ray imaging to evaluate the saturation (Horne et al., 2000) but experiments using capillary pressure method and resistivity data to measure the water saturation

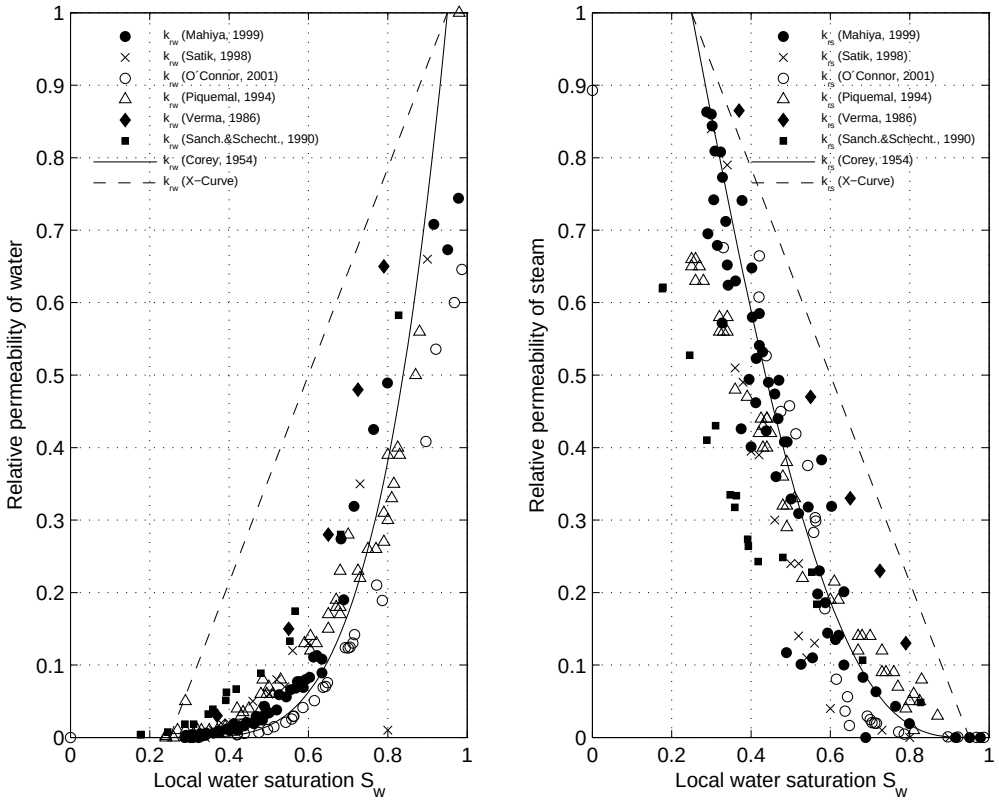

Figure 2.1: Summary of experimental results of relative permeabilities together with the Corey-curve (Corey, 1954) and the X-curve with residual saturations S_{wr}=0.25 and S_{sr}=0.05. Left: Water. Right: Steam.

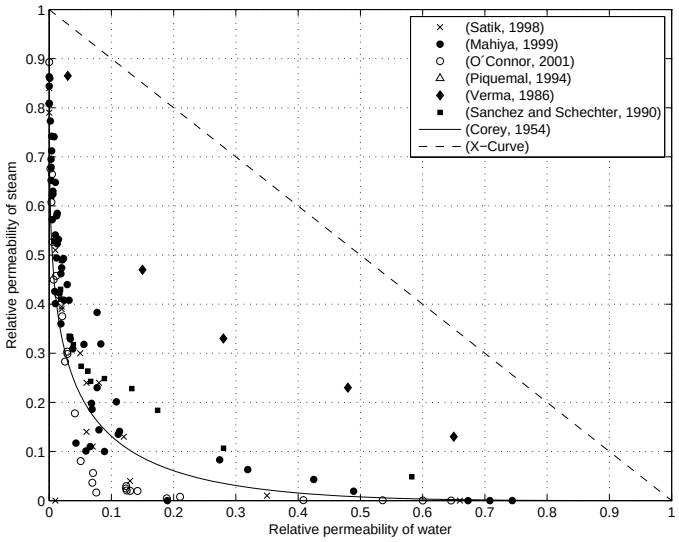

Figure 2.2: Summary of experimental results of relative permeabilities from Fig. 2.1 plotted against each other together with the Corey-curve and the X-curve.

directly have been reported (Li and Horne, 2002), (Li and Horne, 2005a), (Li, 2008), (Li, 2010).

When the local water saturation is not known and can not be measured, like is normally the case for geothermal reservoirs, the flowing water saturation, $S_{w,f}$ which is defined in Eq. (2.20) can be used for comparison.

$$S_{w,f} = \frac{\dot{V}_w}{\dot{V}_w + \dot{V}_s} = \frac{(1-x)v_w}{(1-x)v_w + xv_s} \tag{2.20}$$

where $\dot{V}_w$ and $\dot{V}_s$ are the volumetric flows of water and steam respectively and v_w and v_s are the specific volumes of water and steam respectively and x is the steam fraction as defined in Eq. (2.14). Reyes et al. (2004) found a relation between the local water saturation, S_w, defined in Eqs (2.18) and (2.19) and the flowing water saturation, $S_{w,f}$, defined in Eq. (2.20) which is shown in Eq. (2.21).

$$S_w = 0.1152 \ln(S_{w,f}) + 0.8588 \tag{2.21}$$

By using Eq. (2.21) it is possible to estimate the local water saturation from the flowing saturation and to compare the calculated relative permeabilities to known curves.

2.2.2 Importance of relative permeabilities

The relative permeabilities are not only used to calculate the mass flux or the velocity of the phases but also for estimating thermodynamic and transport properties and they can affect the parameters related to the reservoir performance significantly (Bodvarsson et al., 1980). The total kinematic viscosity ν_t can be calculated from the relative permeabilities and saturation properties as seen in Eq. (2.22) and the flowing enthalpy h_f as seen in Eq. (2.23). These equations can be derived by combining Eqs (2.11) and (2.12).

$$\frac{1}{\nu_t} = \frac{k_{rw}}{\nu_w} + \frac{k_{rs}}{\nu_s} \tag{2.22}$$

$$h_f = \nu_t \left[h_w \frac{k_{rw}}{\nu_w} + h_s \frac{k_{rs}}{\nu_s} \right] \tag{2.23}$$

where ν_w and ν_s are the water and steam kinematic viscosities respectively and h_w and h_s are the water and steam enthalpies respectively.

The importance of relative permeabilities in geothermal reservoir modelling is significant, due to the fact that the flow magnitude of the steam and the enthalpy of the fluid are the key parameters when estimating the thermal energy extracted with the fluid. Choosing appropriate relative permeability functions for the reservoir flow is therefore of great importance in order to avoid overestimation of the reservoir performance (Speyer, 2007).

2.2.3 Relative permeability curves

Various reservoir modelling tools like TOUGH2 (Pruess et al., 1999) and HYDROTHERM (Kipp et al., 2008) have been developed that can be applied to geothermal reservoir flow. There are various relative permeability curves available within these models which describe their relation to the water saturation defined in Eqs (2.18) and (2.19) and the normalized water saturation defined in (2.24).

$$S_{wn} = \frac{S_w - S_{wr}}{1 - S_{sr} - S_{wr}} \tag{2.24}$$

where S_{wr} and S_{sr} are the residual saturation for water and steam respectively.

A sample of relative permeability curves are listed in Table 2.2 all depending on the water saturation. All of the curves, except the X-curves, relate the relative permeabilities to the water saturation as a polynomial with degree 2 or higher. The higher degree of the polynomials in Table 2.2 the more interaction between the two phases is inferred.

In Table 2.2 λ is a function of the pore size distribution index. For the viscous-coupling model $\mu_r = \mu_s/\mu_w$ is the viscosity ratio of the two phases which is small for water and steam flow. λ equals 2 for typical porous media (Chen, 2005) and thereby reduces the Brooks-Corey model to the Corey curves. For fractured media λ reaches infinity (Brooks and Corey, 1966) thus resulting in the Brooks-Corey relations for fractured flow as shown in Table 2.2.

Studies of two phase flow through fractured media have resulted in different relative permeability curves than for flow in porous media. The relative permeabilities were shown to follow the X-Curves in a study by Romm (1966) and results from Diomampo (2001) and Chen (2005) indicated that the relative permeabilities follow the Corey curves.

Table 2.2: A sample of relative permeability functions used in reservoir simulators.

X-Curves:	
$k_{rw} = S_{wn}$	$k_{rs} = 1 - S_{wn}$
Corey Curves (Corey, 1954):	
$k_{rw} = S_{wn}^4$	$k_{rs} = (1 - S_{wn})^2(1 - S_{wn}^2)$
Grants Curves (Grant, 1977):	
$k_{rw} = S_{wn}^4$	$k_{rs} = 1 - k_{rw}$
Functions of Fatt and Klikoff (Fatt and Klikoff, 1959):	
$k_{rw} = S_{wn}^3$	$k_{rs} = (1 - S_{wn})^3$
Functions of Verma (Verma, 1986):	
$k_{rw} = S_{wn}^3$	$k_{rs} = 1.259 - 1.7615 S_{wn} + 0.5089 S_{wn}^2$
Viscous-coupling model (Fourar and Lenormand, 1998):	
$k_{rw} = \frac{S_w^2}{2}(3 - S_w)$	$k_{rs} = (1 - S_w)^3 + \frac{3}{2}\mu_r S_w(1 - S_w)(2 - S_w)$
Brooks-Corey (Brooks and Corey, 1966):	
$k_{rw} = S_{wn}^{(2+3\lambda)/\lambda}$	$k_{rs} = (1 - S_{wn})^2[1 - (S_{wn})^{(2+\lambda)/\lambda}]$
Brooks-Corey for fractured flow:	
$k_{rw} = S_{wn}^3$	$k_{rs} = (1 - S_{wn})^3$
Fracture flow (Sorey et al., 1980):	
$k_{rw} = S_{wn}^4$	$k_{rs} = 1 - S_{wn}^4$

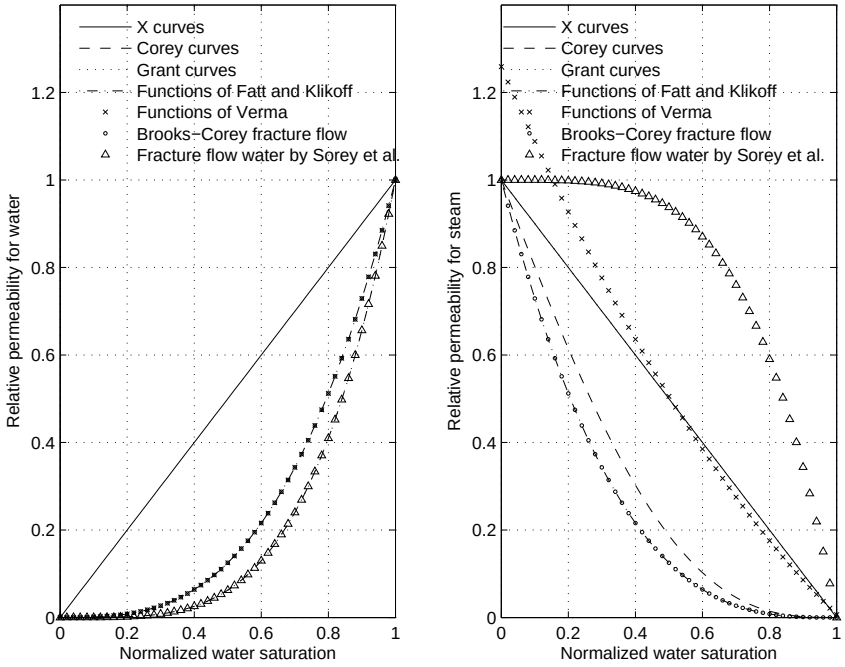

Figure 2.3: Relative permeability curves from Table 2.2 plotted as function of normalized water saturation. Left: Water. Right: Steam

To show the variety of relative permeability curves available, selected curves from Table 2.2 are plotted in Fig. 2.3. It should be noted that the Functions of Verma allow the steam relative permeabilities to exceed 1 but they should always be restricted to be lower than or equal to 1.

Although the main emphasis here is on two phase of water and steam, which are the phases present in hydrothermal reservoirs, much input to this field comes from experiments or field research where there are other substances than water flowing through the porous or fractured material. Some of the relative permeability curves gained from oil and gas experiments, like the Corey curves (Corey, 1954), are widely used for water and steam flow in geothermal reservoir modelling.

2.3 Application of Darcy's law to geothermal reservoirs

Flow in porous or fractured rocks in high temperature geothermal systems occurs under different conditions as seen in Chapter 1. One example is where groundwater flows into the system, and another where geothermal fluid gains heat in the system due to conduction from a magmatic heat source below. One more example is the

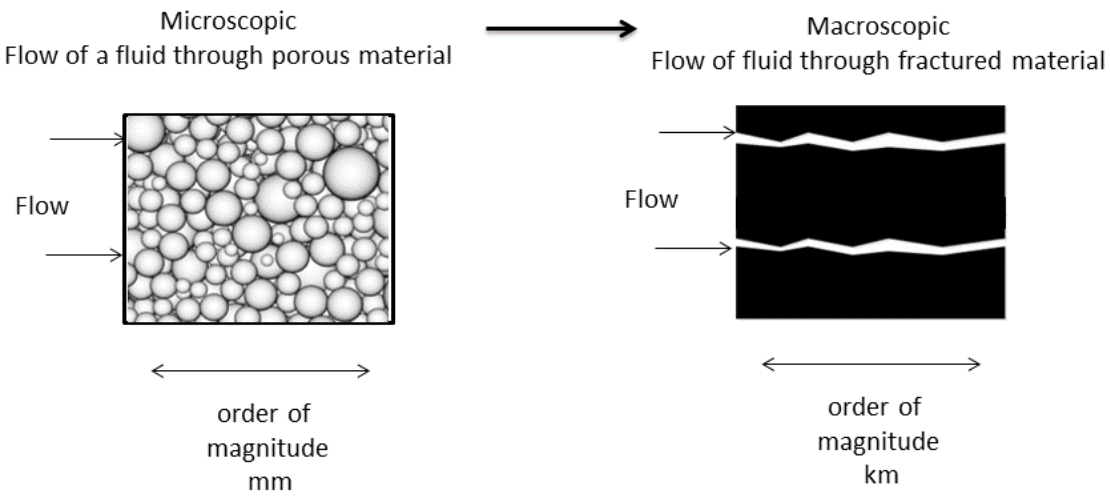

Figure 2.4: Representation of how Darcy's law is applicable for small scale porous material as well as large scale fractured material.

flow towards wells which have been drilled into the geothermal system.

Geothermal reservoirs normally consist of fractured media where the reservoir fluid flows through fractures rather than homogeneous porous and permeable material (Grant and Bixley, 2011). Darcy's law is applicable on a microscopic scale for a flow of fluid through porous medium like small grained material but research indicates that it can also to be applicable to a macroscopic scale like fractured material (Chen, 2005), see Fig. 2.4. Therefore Darcy's law is generally used to model flow through fractured geothermal reservoirs.

A method introduced by Shinohara (1978) enables the determination of the relative permeabilities of water and steam in a geothermal reservoir using production history and enthalpy measurements for a geothermal well drilled into the reservoir. By using Eqs (2.11) and (2.12) (assuming one dimensional, horizontal flow neglecting gravity effect and rearranging terms) we get the following:

$$k_{rw} = -\frac{\dot{m}_w \nu_w}{kA\nabla p} = \frac{\dot{m}_w \nu_w}{Q^* \nu_s} \tag{2.25}$$

$$k_{rs} = -\frac{\dot{m}_s \nu_s}{kA\nabla p} = \frac{\dot{m}_s}{Q^*} \tag{2.26}$$

where:

$$Q^* = -\frac{kA\nabla p}{\nu_s} \tag{2.27}$$

The total mass flow, $\dot{m}_t$ of the two phase mixture according to Eqs (2.11) and (2.12) is:

$$\begin{aligned}\dot{m}_t = \dot{m}_w + \dot{m}_s &= -kA\nabla p\left(\frac{k_{rw}}{\nu_w} + \frac{k_{rs}}{\nu_s}\right) \\ &= -kA\nabla p\frac{k_{rs}}{\nu_s}\left(\frac{k_{rw}}{\nu_w}\frac{\nu_s}{k_{rs}} + 1\right) = Q^* k_{rs}\left(\frac{\dot{m}_w}{\dot{m}_s} + 1\right)\end{aligned} \tag{2.28}$$

When applying the Shinohara method on the well data from a geothermal field, the total discharge $\dot{m}_t$ has to be known. Furthermore to determine the mass flow ratio $\dot{m}_w/\dot{m}_s$ at downhole conditions the enthalpy of the fluid h_t has to be known and the steam fraction of the two phase mixture can be determined by Eq. (2.17). The steam fraction in the two phase reservoir from Eq. (2.17) can then be used to determine the mass flow of each phase in the reservoir to the well using the total flow rate $\dot{m}_t$ as seen in Eqs (2.15) and (2.16).

Now if $\dot{m}_w = 0$ then $k_{rs} = 1$ and according to Eq. (2.28) Q^* can be found by plotting $\dot{m}_t$ against $\dot{m}_w/\dot{m}_s$ since Q^* is the intercept to y-axis of the regression line, as demonstrated in Fig. 2.5. To plot this figure for a production well, a production history of the total mass flow from the well as well as the ratio of the mass flows of the two phases have to be available.

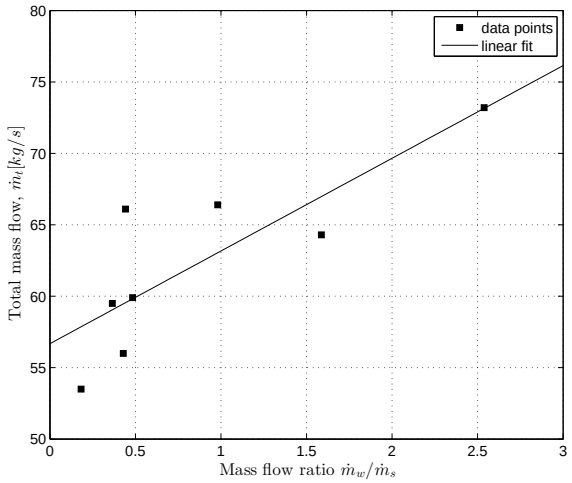

Figure 2.5: Representation of how to determine the parameter Q^* for the Shinohara method for an arbitrary well. Q^* is the value where the regression line intercepts the y-axis as seen from Eq. (2.27).

The assumptions made for using the Shinohara method on a geothermal well to determine the relative permeabilities of the two phases in the reservoir, are the following (Shinohara, 1978):

- The pressure gradient is constant for a short time for each well

- The product of permeability and flowing area, kA, is constant for each well
- Wellhead steam and water discharges are the same as downhole values, thus neglecting flashing of fluid in the wellbores
- Fluid flows in the reservoir according to Darcy's law
- Flashing in the reservoir is neglected

Also, it is assumed that the flow in the two phase reservoir is horizontal, that is without effect from gravity in the momentum balance.

In reality, the two phase fluid will flash in the reservoir and in the well due to decreasing pressure and part of the liquid water will transform into steam. The downhole steam and water discharges are therefore different than at the wellhead. If the downhole properties (that is the temperature and therefore the fluid viscosity and density) are known, a correction to account for flashing in the well can be made. The downhole properties are used to estimate the steam fraction, x, at the bottom of the well at the given enthalpy h_t which is assumed to be constant in the well. Thus a better approximation for the mass flow ratio is gained for the downhole conditions based on the estimated steam fraction. By obtaining Q^* from Eq. (2.27) and a plot like is shown in Fig. 2.5 as well as the total flow and the mass fraction (which can be determined if the total enthalpy of the flow is known), k_{rw} and k_{rs} can be determined according to Eqs (2.25) and (2.26).

The relations shown in this Chapter 2 are suited for analysis of Darcy's law and applying it to measured data from laboratory experiments and field data. Like stated in Section 1.2 the primary purposes of this research were to study directional dependency of the relative permeabilities in liquid dominated systems and to estimate the relative permeabilities in experiments using geothermal fluid and to compare it to field data. The methods, materials and the key results of the scientific papers that were written in this project and are appended to this thesis are described in the next Chapter 3.

3 Methods, materials and key results

3.1 Paper I

The effect of gravity on the application of relative permeabilities in modelling two phase geothermal reservoirs

3.1.1 Introduction

This study refers to the research described in Paper I which is appended to this thesis. The subject was to analyse the effect of gravity on the relative permeabilities. Starting with Eqs (2.11) and (2.12), these equations were simplified to represent one dimensional flow for two cases. One case was horizontal flow where the fluid flow was perpendicular to gravity and the other case was vertical flow where the fluid flow was parallel to and against the gravitational acceleration. By eliminating the pressure gradient $^{\Delta p}/_{\Delta x}$ from Eqs (2.11) and (2.12), and using the steam fraction from Eq. (2.14) the following Eqs (3.1) and (3.2) were obtained for each flow case.

$$\left(\frac{\Delta p}{\Delta x}\right)_{hor} = -\frac{x\dot{m}_t\nu_s}{kk_{rs}A} = -\frac{(1-x)\dot{m}_t\nu_w}{kk_{rw}A} \tag{3.1}$$

$$\left(\frac{\Delta p}{\Delta x}\right)_{ver} = -\frac{x\dot{m}_t\nu_s}{kk_{rs}A} - \rho_s g = -\frac{(1-x)\dot{m}_t\nu_w}{kk_{rw}A} - \rho_w g \tag{3.2}$$

where the subscripts *hor* and *ver* refer to horizontal and vertical flow direction respectively. $\dot{m}_t$ is the total mass flow of the two phase mixture according to Eq. (3.3).

$$\dot{m}_t = \dot{m}_w + \dot{m}_s \tag{3.3}$$

The two equations Eqs (3.1) and (3.2) can be rewritten as Eqs (3.4) and (3.5).

$$\left(\frac{k_{rs}}{k_{rw}}\right)_{hor} = \frac{x}{(1-x)}\frac{\nu_s}{\nu_w} \tag{3.4}$$

$$\left(\frac{k_{rs}}{k_{rw}}\right)_{ver} = \frac{x}{(1-x)}\frac{\nu_s}{\nu_w} + \frac{k_{rs}gk(\rho_s - \rho_w)}{(1-x)\frac{\dot{m}_t}{A}\nu_w} \tag{3.5}$$

If the widely used Corey curves from Table 2.2 are used as the relative permeability functions and inserted into Eqs (3.4) and (3.5), the normalized saturation $S_{wn,hor}$ can be solved from Eq. (3.6) for the horizontal flow and $S_{wn,ver}$ from Eq. (3.7) for the vertical flow.

$$\frac{(1-S_{wn,hor})^2(1-S_{wn,hor}^2)}{S_{wn,hor}^4} = \frac{x}{1-x}\frac{\nu_s}{\nu_w} \tag{3.6}$$

$$\begin{aligned}&\frac{(1-S_{wn,ver})^2(1-S_{wn,ver}^2)}{S_{wn,ver}^4} \\ &= \frac{x}{1-x}\frac{\nu_s}{\nu_w} + \frac{(1-S_{wn,ver})^2(1-S_{wn,ver}^2)gk(\rho_s-\rho_w)}{(1-x)\frac{\dot{m}_t}{A}\nu_w}\end{aligned} \tag{3.7}$$

Now, Eqs (3.6) and (3.7) have only one unknown parameter each ($S_{wn,hor}$ and $S_{wn,ver}$ respectively) for a given flow case where $\dot{m}_t$, A, k x, ν and ρ are known instead of two parameters (k_{rw} and k_{rs}) in each of Eqs (3.4) and (3.5).

Consequently, by inserting the resulting normalized saturation from Eqs (3.6) and (3.7) into the Corey curves the corresponding relative permeabilities for the horizontal and the vertical flow case can be determined. Then, the difference in relative permeabilities between the flow cases in Eq. (3.4) and Eq. (3.5) can be quantified.

The mass flux $\frac{\dot{m}_t}{A}$ has however to be determined to get further with Eq. (3.7). It was estimated from a simplified convection cell which was used to represent a geothermal reservoir as described in the next Section 3.1.2.

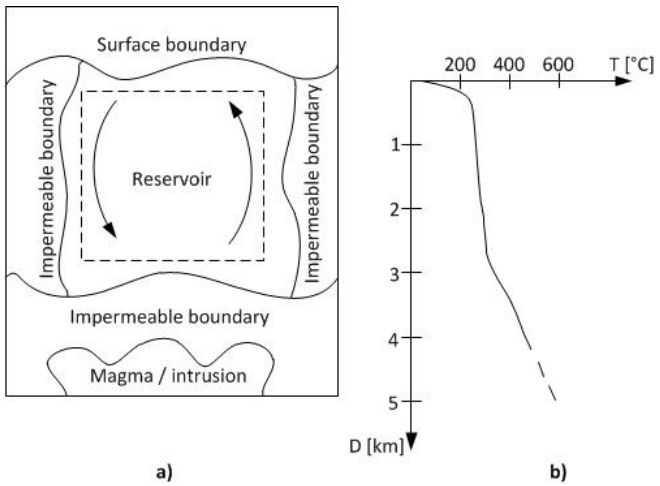

Figure 3.1: a) Convective system representing a convective volcanic geothermal reservoir b) A typical temperature (T) vs. depth (D) profile for a convective geothermal system (Axelsson, 2008).

3.1.2 Mass flow estimate in a convection cell

The concept of a convection cell is a simplification of the fluid flow and the heat transfer through a convective geothermal reservoir as shown schematically in Fig. 3.1a. The heat transfer occurs by different mechanisms through different layers in the geothermal reservoir as described by White (1967) and was described in Section 1.1. Temperature gradients for the layers are demonstrated by the example of a temperature vs. depth profile in Fig. 3.1b.

This behaviour can be described by a simplified convection cell with a streamline for the geothermal fluid in a circuit spanning a vertical height L as demonstrated in Fig. 3.2. Note that the three terms (which are forces per unit volume) on each side of the cell are in balance. If the flow through the convection cell can be assumed to follow Darcy's law, the momentum balance for the fluid gives:

$$\vec{f_\nu} + \vec{f_g} + \nabla p = \frac{\vec{m}}{A}\frac{\nu}{k} + \rho\vec{g} + \nabla p = 0 \tag{3.8}$$

If the terms in Eq. (3.8) are integrated along the streamline, s, and around the cell

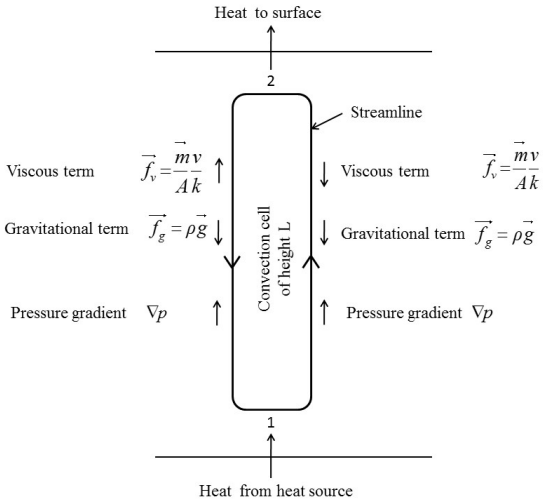

Figure 3.2: Convection in a geothermal reservoir described by a simplified convection cell and the corresponding terms according to Darcy's law in Eq. (2.1).

(see Fig. 3.2) Eq. (3.9) is obtained.

$$\begin{aligned} &\oint \vec{f}_\nu \cdot d\vec{s} + \oint \vec{f}_g \cdot d\vec{s} + \oint \nabla p \cdot d\vec{s} \\ &= \oint \frac{\vec{m}}{A}\frac{\nu}{k} \cdot d\vec{s} + \oint \rho\vec{g} \cdot d\vec{s} + \oint \nabla p \cdot d\vec{s} = 0 \end{aligned} \tag{3.9}$$

The circular integral of the pressure gradient becomes zero. Assuming that the horizontal sections of the convection cell are negligibly small, the integrals between conditions 1 and 2 and 2 and 1 shown in Fig. 3.2 for the other terms become:

$$\int_1^2 \vec{f}_\nu \cdot d\vec{s} + \int_2^1 \vec{f}_\nu \cdot d\vec{s} + \int_1^2 \vec{f}_g \cdot d\vec{s} + \int_2^1 \vec{f}_g \cdot d\vec{s} = 0 \tag{3.10}$$

When integrated over the height of the convection cell L, the resulting terms in Eq. (3.10) become:

$$-\frac{\dot{m}\nu_1}{Ak}L - \frac{\dot{m}\nu_2}{Ak}L - \rho_1 gL + \rho_2 gL = 0 \tag{3.11}$$

Finally the resulting mass flux for a flow in a convection cell as demonstrated in

Fig. 3.2 becomes:

$$\frac{\dot{m}}{A} = \frac{(\rho_2 - \rho_1)gk}{(\nu_1 + \nu_2)} \tag{3.12}$$

In Eq. (3.12) ρ_1 is the average density on the way up the convection cell and ρ_2 is the density of saturated water on the way down the convection cell.

Many simplifications are made in this context to obtain this rough estimate of the mass flux. Here it is assumed that the mass flux is constant through the convection cell which is generally not the case for real geothermal reservoirs.

3.1.3 Ratio of phase velocities

In the case of a two phase flow the flow velocities may not be the same for both phases. Different velocity ratios for the phases between the two flow cases would indicate that there are different water saturations for the two cases if other properties are identical. By using the results for the normalized water saturations in the previous section the ratio of the two phase velocities can now be calculated. In case of one dimensional two phase flow, the flow areas of the two phases can be determined by the water saturation which is used to determine the local velocities of the two phases by inserting it into Eqs (3.13) and (3.14).

$$v_w = \frac{\dot{m}_w}{\rho_w S_w A} \tag{3.13}$$

$$v_s = \frac{\dot{m}_s}{\rho_s (1 - S_w) A} \tag{3.14}$$

This leads to the phase velocity ratio as defined in Eq. (3.15).

$$\frac{v_s}{v_w} = \frac{x \rho_w S_w}{(1 - x)\rho_s (1 - S_w)} \tag{3.15}$$

The velocity ratios can then be determined from the calculated normalized water saturation, using residual saturations for each phase according to Eq. (2.24). The ratio can then be calculated for each direction, horizontal and vertical for known flowing steam fraction, x.

3.1.4 Modelling two phase reservoir flow

The estimate for the specific mass flow shown in Eq. (3.12) can now be used in Eq. (3.5) to estimate the relative permeabilities for water and steam for the vertical flow direction. The method described above was applied for a specific flow case. Flow of water and steam was simulated and the mass flux was estimated from flow in a simple convection cell model within a reservoir with intrinsic permeability $k = 1$ Darcy. This method was applied for specific flow cases, starting with a saturated liquid at a given pressure and steam fraction $x = 0$. The pressure decreases along the flow path thus driving the flow onwards from the initial point in the flow path with pressure $p_{in} = 100$ bar and steam fraction $x = 0$. For each flow case, the fluid flashes adiabatically along the flow path. Here adiabatic flow can be assumed since this simulates a steady state flow in a geothermal reservoir where the rock temperature has reached equilibrium with the reservoir fluid. The fluid flows and flashes along the way to an end point with pressure $p_{end} = 50$ bar. The total length of the flow path in each flow case can differ, since the pressure gradients $(\frac{\Delta p}{\Delta x})_{hor}$ and $(\frac{\Delta p}{\Delta x})_{ver}$ in Eqs (3.1) and (3.2) can differ. Based on the pressure, the saturation enthalpies h_w and h_s can be determined since h_t is constant (saturated liquid at the initial pressure). The steam fraction can be determined from Eq. (2.17) in the flow path as well as other thermodynamic and transport properties.

Now, since the properties are known along the flow path as described above, the corresponding normalized water saturations in Eqs (3.6) and (3.7) can be determined. Consequently, by inserting the resulting normalized saturation from Eqs (3.6) and (3.7) into the Corey curves the corresponding relative permeabilities and velocity ratios for the horizontal and the vertical flow cases can be determined.

3.1.5 Summary of results and discussion

The relative permeabilities were calculated using Eqs (3.4) and (3.5) for the two cases, horizontal flow and vertical flow opposite to gravity. The Corey curves were selected as the relative permeability functions and the normalized saturations solved numerically from Eqs (3.6) and (3.7). The phase velocity ratios were also calculated using Eq. (3.15).

As seen in Eq. (3.5) the mass flux $\frac{\dot{m}_t}{A}$ in Eq. (3.5) needs to be determined first. In this study, the mass flux was estimated from flow in a simple convection cell model, as described in Section 3.1.2, within a reservoir with intrinsic permeabiliy $k = 1$ Darcy.

Fig. 3.3 shows the resulting normalized water saturations (left) and the relative

permeabilities (right) of water and steam versus the steam fraction for the two flow directions that were modelled. The initial pressure of the saturated liquid was 100 bar (where the steam fraction was $x = 0$) and the fluid flashed down to 50 bar (where the steam fraction was $x = 0.155$) which resulted in total mass flux of $0.0144\frac{kg}{m^2 s}$.

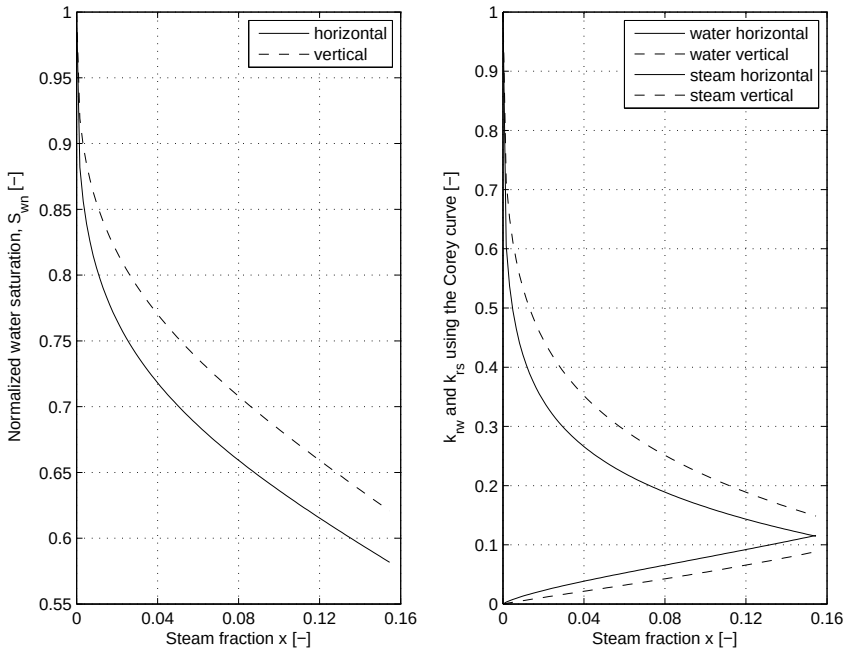

Figure 3.3: Left: Normalized water saturation for horizontal and vertical flow cases as functions of steam fraction, with a total mass flux of $0.0144\frac{kg}{m^2 s}$. *Right: Relative permeabilities according to Corey curves for water and steam as functions of steam fraction for two flow alignments and total mass flux of* $0.0144\frac{kg}{m^2 s}$.

The sensitivity of the normalized saturations and the relative permeabilities to mass flux is shown in Figs 3.4 and 3.5. In Fig. 3.4 the mass flux is 10 times the initial mass flux used for the calculations in Fig. 3.3 and in Fig. 3.5 the mass flux is one tenth of the mass flux in Fig. 3.3. It can be seen, that higher mass flux results in less difference between the horizontal and vertical relative permeabilities whereas lower mass flux results in greater difference.

The phase velocity ratio defined in Eq. (3.15) was then calculated and is shown in Fig. 3.6 together with the sensitivity to the mass flux. The residual saturations used to gain the local water saturations from the normalized saturations were S_{sr}=0.05 and S_{wr}=0.25. It is not known from the literature if the residual saturations depend on the flow direction. In Fig 2.1 the only experiment performed on a fluid flowing inclined from horizontal was in the study by Verma (1986). In that study the flow direction was opposite to gravitational acceleration and the residual saturations are reported as S_{sr}=0.105 and S_{wr}=0.2. The sensitivity of the velocity ratios to the residual saturations is shown in Fig. 3.7 where the residual saturations for the

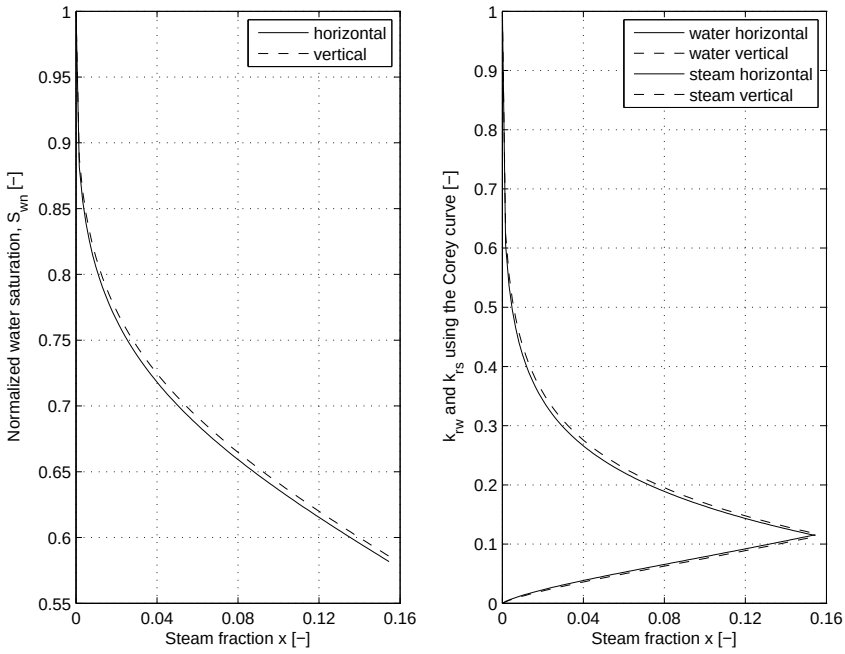

Figure 3.4: Left: Normalized water saturation for horizontal and vertical flow cases as functions of steam fraction with 10 times the mass flux used in Fig. 3.3. Right: Relative permeabilities according to Corey curves for water and steam as functions of steam fraction for two flow alignments with 10 times the mass flux as calculated for in Fig. 3.3.

horizontal flow case are constant but vary for the vertical flow case.

When Darcy's law is applied to two phase flow of water and steam in geothermal reservoirs, different relative permeabilities are observed, depending on the flow direction. This difference has been quantified in this section for a particular set of relative permeability functions and a specific flow model. The method described here, enables solving of the normalized water saturation and calculate the corresponding relative permeabilities using a selected set of curves. This method was applied to two flow cases which differed only in flow direction against gravity. The results show that there can be a significant difference in the water saturation and correspondingly in the relative permeabilities between the two cases although they share properties like steam fraction, enthalpy, pressure, viscosity and temperature. The difference is mainly due to the reluctance of the heavier phase, water, to flow upwards against gravity. As shown in Eqs (2.6) and (2.7) the weight of the hydrostatic column acts against the flow and therefore the heavier the phase is, the more difficult it is for the phase pressure gradient to exceed it and to enable its upward flow. Therefore, as seen in Figs 3.3 to 3.5, the relative permeabilities for water have higher values for the vertical flow than the horizontal flow for the same steam fraction since they occupy more area there. On the other hand, the steam has

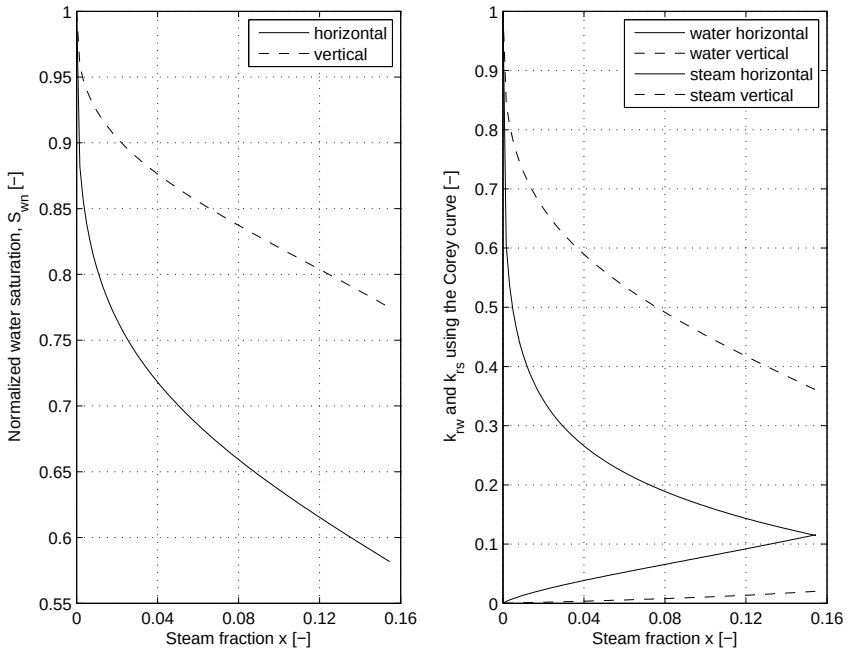

Figure 3.5: Left: Normalized water saturation for horizontal and vertical flow cases as functions of steam fraction with 0.1 times the mass flux used in Fig. 3.3. Right: Relative permeabilities according to Corey curves for water and steam as functions of steam fraction for two flow alignments with 0.1 times the mass flux as calculated for in Fig. 3.3.

lower relative permeabilities for vertical flow as for the horizontal flow for the same steam fraction, since the area of the flow channel containing steam is smaller there. Higher phase velocity ratios are obtained for the vertical flow case as compared to the horizontal flow case. This is shown in Fig 3.6 where the phase velocity ratios are plotted as a function of the steam fraction, x, for a range of mass flow rates. The difference of the phase velocities between flow alignments therefore explains the difference in normalized water saturations and the relative permeabilities. The sensitivity of the phase velocity ratios to residual saturations are shown in Fig. 3.7 where the residual saturations for the horizontal flow is constant and the residual saturations for the vertical flow varies.

3.1.6 Conclusions of Paper I

Two flow cases were considered, one where flow of water and steam flowed perpendicular to gravitational acceleration, and other where they flowed opposite to it. By applying known relative permeability functions (Corey curves) into Darcy's law, the water saturations and correspondingly the relative permeabilities could be solved

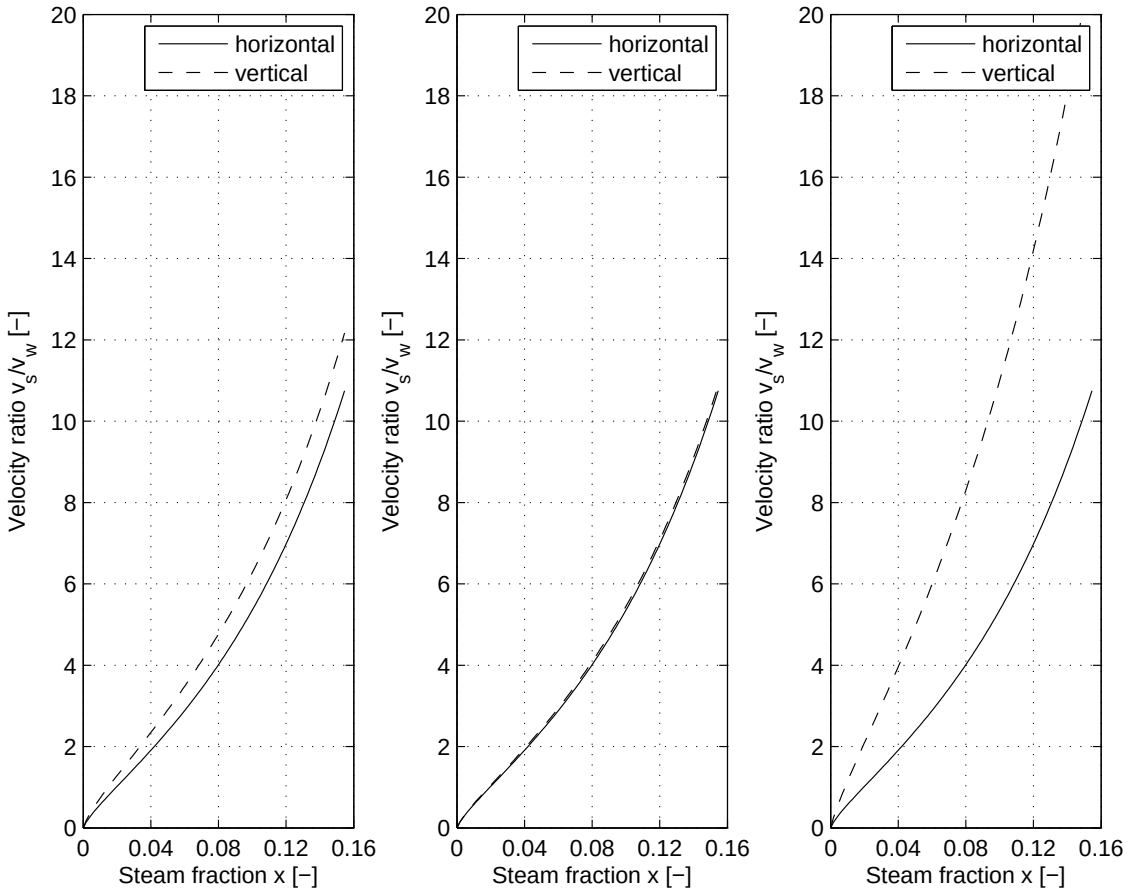

Figure 3.6: Left: Velocity ratios according to Corey curves for water and steam as functions of steam fraction for two flow alignments.
Middle: Velocity ratios with 10 times the mass flux as calculated for in Left.
Right: Velocity ratios with 0.1 times the mass flux as calculated for in Left.

for both cases. The resulting relative permeabilities are different between the two cases, although the properties are the same. The magnitude of the flow alters this difference. The phase velocity ratios which were also calculated differ as well between the flow cases, which can explain the difference in the water saturations and the relative permeabilities.

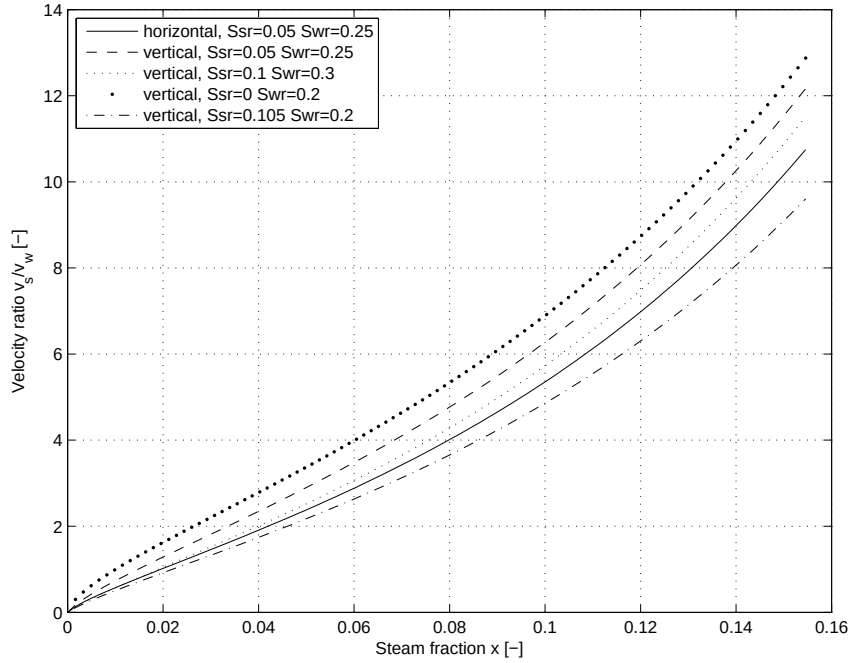

Figure 3.7: The sensitivity of velocity ratios for the vertical flow alignment with the flow rate as in the left part of Fig. 3.6 to the residual saturations.

3.2 Paper II

Water and air relative permeabilities from laboratory experiments. The effect of flow direction.

3.2.1 Introduction

This study refers to the research described in Paper II which is appended to this thesis. Darcy's law from Eqs (2.4) and (2.5) from Section 2.1.2 were used for a two phase flow of water and air. The purpose of this study was to observe the effect of gravity on the relative permeabilities of the two phases like discussed in Section 3.1. Experiments were conducted on a water and air mixture which flowed through porous media which consisted of uniform glass beads. The main advantage using phases of different substances is that one phase does not convert to the other so that the mass fraction is constant through the porous flow channel under observation.

For water and air mixture Eqs (2.4) and (2.5) become Eqs (3.16) and (3.17) when

same pressure gradients apply to both phases.

$$\vec{q_w} = -\frac{kk_{rw}}{\nu_w}(\nabla p - \rho_w \vec{g}) \tag{3.16}$$

$$\vec{q_a} = -\frac{kk_{ra}}{\nu_a}(\nabla p - \rho_a \vec{g}) \tag{3.17}$$

where the subscripts w and a represent the water and the air respectively. x_a is the mass fraction of air as defined in Eq. (3.18).

$$x_a = \frac{\dot{m}_a}{\dot{m}_a + \dot{m}_w} \tag{3.18}$$

Two phase flow of water and air was used in experiments in order to validate the results derived from theoretical relations in Section 3.1.

3.2.2 Experimental procedure

An experimental device was designed and installed to use for the water-air relative permeability measurements. A process diagram and a photo of the device are shown in Fig. 3.8. The equipment numbers shown in the process diagram refer to the equipment list shown in Table 3.1. The pipe (component C in Table 3.1) was filled with porous material which was packed glass beads with grain size 125-850 μm (COPRO, 2014) and connected to air and water inlets which were controlled with valves (components A). Flow rate of air was measured at the pipe inlet (component B) and then the air was mixed with water before entering the inlet of the tube (condition 3 in Fig. 3.8). The pressure inside the pipe was measured at two locations (components D) with ΔL distance between them, thus enabling the calculation of the pressure gradient. At the outlet of the pipe, backpressure could be controlled with a valve (component E). The two phase mixture at the outlet was then separated in air-water separator (component F) thus enabling measurements of the water flow rate (component G). The temperature of the water was measured at the outlet (component H) enabling determination of the fluid properties like viscosity which can be highly temperature dependant.

First, water was used alone to flow through the porous filling in order to calculate the intrinsic permeability using Eq. (2.1). Water and air mixture was then driven through the porous filling, for varying mass ratios and pressures. Since the flow

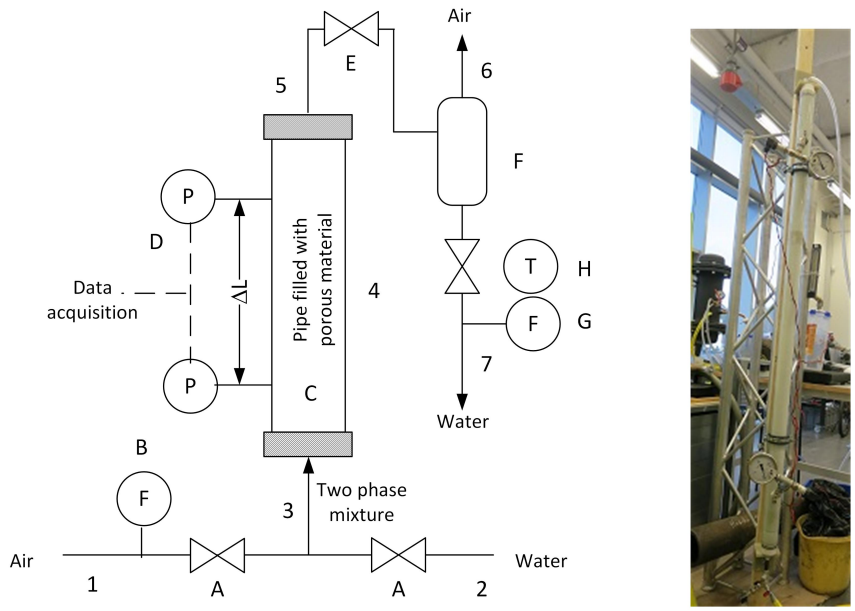

Figure 3.8: Left: Process diagram for the air-water experiments. Right: Setup of the air-water experiment.

rates, the intrinsic permeability, the pressure gradient and the viscosity and density of each phase was known, the relative permeabilities could be calculated from Eqs (3.16) and (3.17). This was repeated for the two flow directions, horizontal and vertical.

Table 3.1: Description of the components of the measurement device. Letters refer to Fig. 3.8. D = diameter, t = thickness, L = length.

Component	Name	Description
A	Valve	D=1/8 inch
B	Air flow meter	Rotameter
C	Pipe filled with glass beads	D = 6 cm, t = 3 mm, L = 172 cm, plexyglass pipe
D	Pressure sensor / Indicator	Tecsis 4-20 mA Tecsis (2015) / indicator
E	Back pressure valve	D=1/2 inch
F	Air-water separator	
G	Water flow meter	Mass and time measurements
H	Temperature measurement	

3.2.3 Summary of results and discussion

The intrinsic permeability values were measured between the two-phase runs and resulted in values ranging from 40-54 Darcy. The intrinsic permeability value that was used for the relative permeability calculations was the value obtained before the specific two-phase run. Fig. 3.9 shows the results from the relative permeability calculations using the measured values. The Corey curves from Table 2.2 are also shown on the graphs.

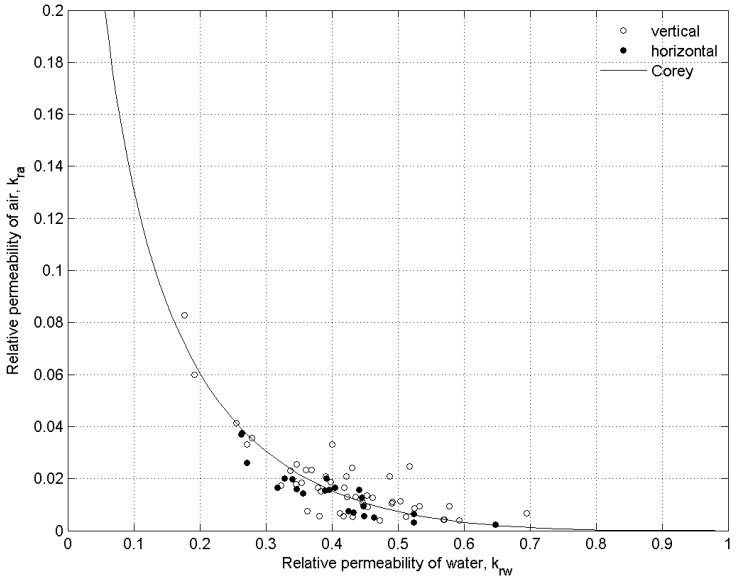

Figure 3.9: Results of relative permeabilities calculated from measured values together with the Corey curves.

Fig 3.10 shows the relative permeabilities of water and air respectively versus the mass fraction of air calculated with Eq. (3.18). The relative permeabilities for the vertical flow case were classified into groups with respect to the flow rates as shown in the figures using different legends. Low flow rate refers to the data points where the mass flow rate was less than 2 g/s and high mass flow rate where the mass flow rate was above 2 g/s.

To evaluate if there is a difference in the behaviour of the three groups (horizontal flow, vertical flow with low flow rate and vertical flow with high flow rate) in Fig. 3.10 a linear regression analysis was made. A linear regression line was fitted through the datasets for the groups, as shown in Fig. 3.11. On the left side in Fig. 3.11 the water relative permeabilities are plotted against the logarithm of the mass fraction of air and on the right side air relative permeabilities are plotted against the logarithm of the mass fraction of air. The mean and the standard error of the slope and the

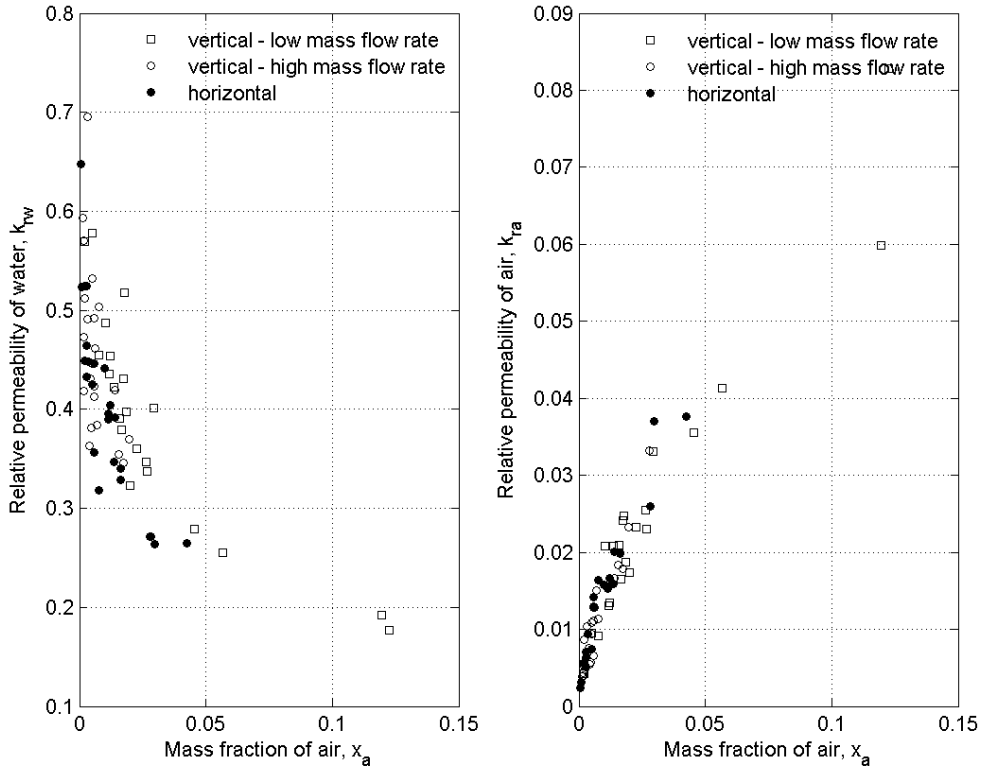

Figure 3.10: Left: Results of the relative permeabilities for water in relation to the mass fraction of air.
Right: Results of the relative permeabilities for air in relation to the mass fraction of air.

intercepts of the regression lines shown in Fig. 3.11 are shown in Fig. 3.12 for water and Fig. 3.13 for air. For the air relative permeabilities in the right hand side of Fig. 3.11 the two datapoints with the highest air relative permeabilities were omitted from the linear regression analysis since they change greatly the slope of the trendline of the vertical flow case with low flow rate.

Fig 3.14 shows the calculated relative permeabilities using Eqs (3.4) and (3.5) using the Corey curves as the relative permeability curves to solve the normalized water saturation from them and calculate the relative permeabilities. The measured values are also shown in Fig 3.14 for comparison. For calculating the relative permeabilities using Eqs (3.4) and (3.5) the mass fraction, density and viscosity from the measurements were used. The pressure gradient were not needed for those calculations.

Fig. 3.9 shows that the relative permeabilities from measured values follow the Corey curves to some extent. Fig. 3.10 indicates that when the flow rate of vertical

flow alignment is low, the relative permeabilities deviate more from the relative permeabilities of the horizontal flow alignment than when the flow rate is high. This can also been seen from the trendlines that were fitted to the data as shown in Fig. 3.11 and analysis of slope and intercept of the trendlines shown in Figs 3.12 and 3.13.

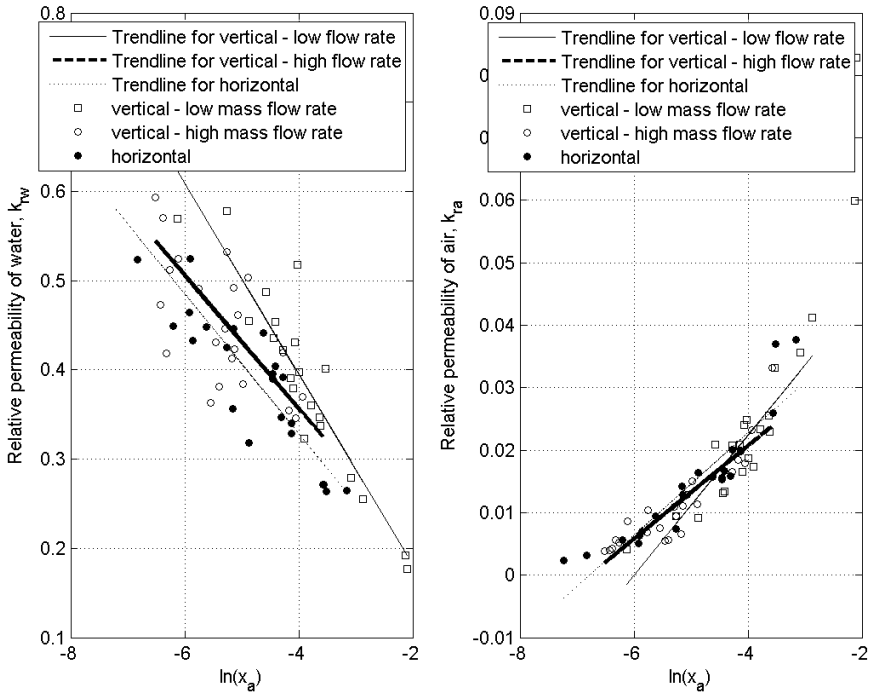

Figure 3.11: Regression lines fitted through the data set for water (left) and air (right).

The results of the linear regression for water shown in Fig. 3.12 indicate the tendency of the relative permeabilities for vertical flow case with low mass flow rates to deviate from the other two. This is also observed for air as shown in Fig. 3.13. There is some scattering in the data points and error factors in the measurements are various. There is some variance in the intrinsic permeabilities due to the fact that the porous media was not consolidated so a homogeneous packing could not be assured. A rotameter was used for air flow measurements and some measurement errors are expected there.

Fig. 3.14 shows the comparison of the relative permeabilities using directly measured values and Eqs (3.16) and (3.17) and the calculated relative permeabilities gained using Eqs (3.4) and (3.5) using the Corey curves. Clearly, the relative permeabilities found using the two methods show similar trend.

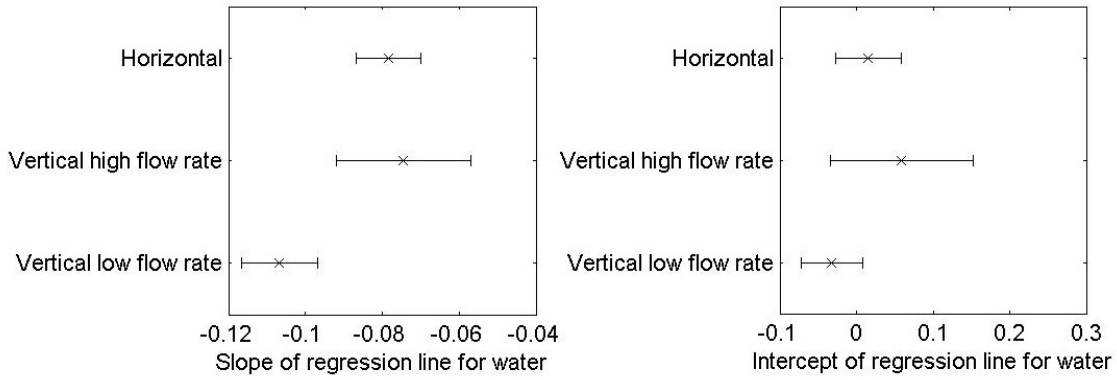

Figure 3.12: Mean and standard error of the slope (left) and the intercept (right) of the regression line for the water relative permeabilities shown in the left part in Fig. 3.11.

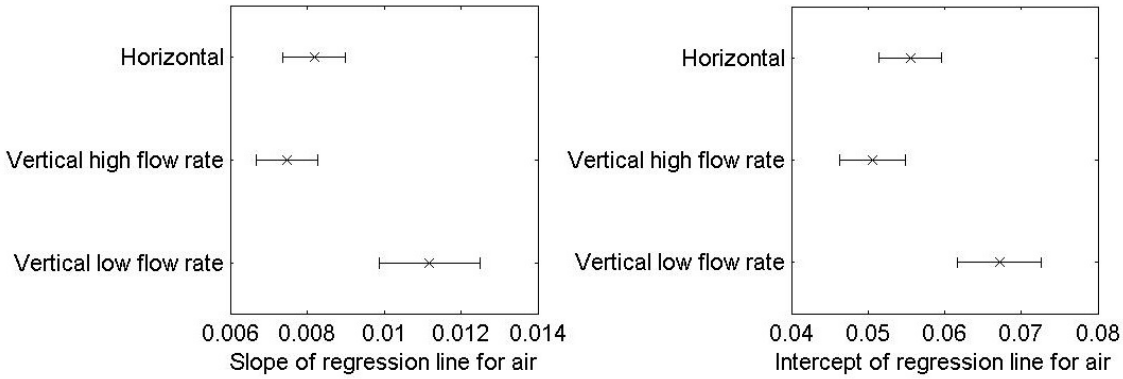

Figure 3.13: Mean and standard error of the slope (left) and the intercept (right) of the regression line for the air relative permeabilities shown in the right part in Fig. 3.11.

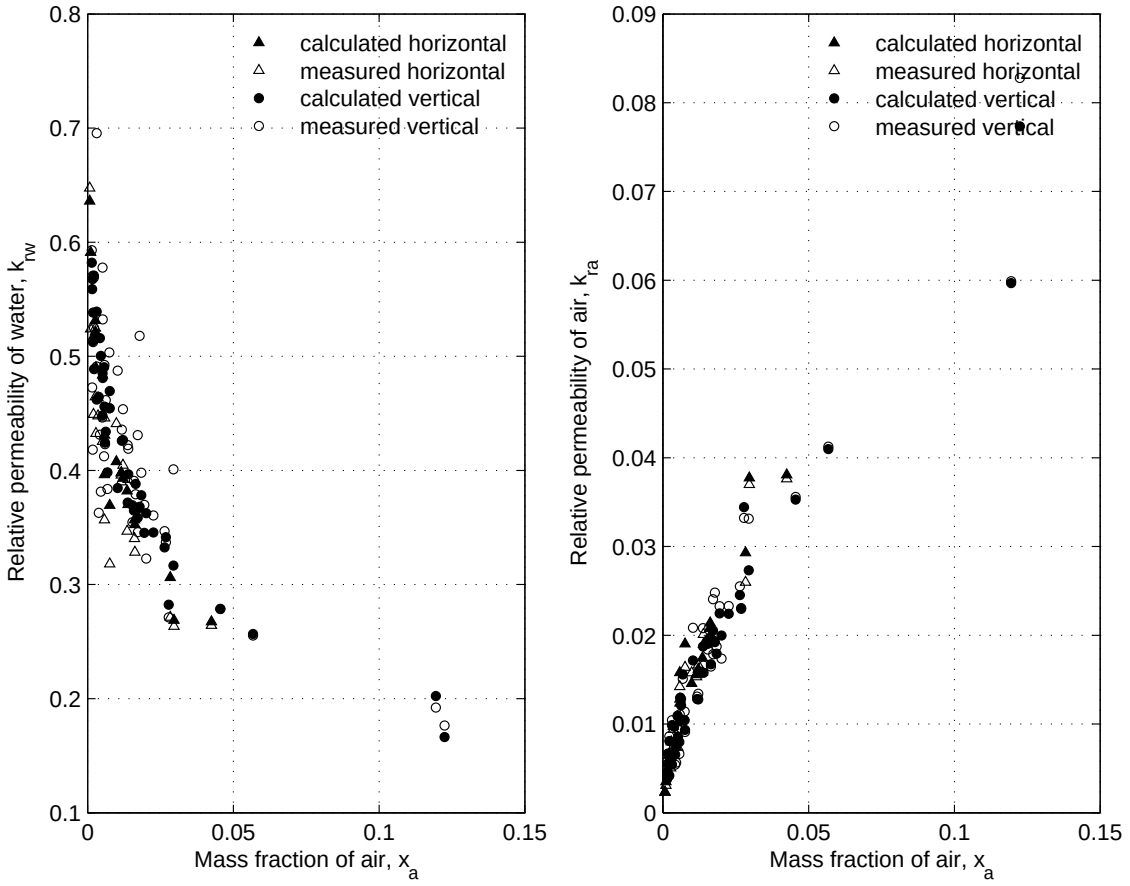

Figure 3.14: Left: Comparison of the calculated and the measured values of water relative permeability in relation to the mass fraction of air.
Right: Comparison of the calculated and the measured values of air relative permeability in relation to the mass fraction of air.

3.2.4 Conclusions of Paper II

The analysis of Darcy's law shown in Paper I is supported in this study by laboratory measurements using water and air. The relative permeabilities were calculated from directly measured parameters and followed the Corey curves to some extent. A difference in the relative permeabilities was observed with regard to flow direction and flow magnitude which was also the case in Paper I.

3.3 Paper III

Calculations of relative permeabilities of water and steam from laboratory measurements

3.3.1 Introduction

This study refers to the research described in Gudjonsdottir et al. (2015b) which is appended to this thesis. The flow of a geothermal fluid through a geothermal reservoir resembles flow through porous material with Darcy's law as one of the governing equations. In reality, geothermal reservoirs normally consist of fractured rock with the inhomogeneous permeability of a fractured matrix (Grant and Bixley, 2011). On a macroscopic scale, the porous media assumption seems appropriate (Chen et al., 2004), (Chen and Horne, 2006) and it is conventionally used to describe flow in geothermal reservoirs (Chen, 2005) although some reservoir modelling tools like TOUGH2 allow double porosity and dual permeability definitions for the reservoir structure (Pruess et al., 1999).

As stated in Chapter 1 the relative permeabilities are important parameters in reservoir modelling. They are not only used to calculate the mass flux or the velocity of the phases but also for estimating thermodynamic and transport properties and can affect the parameters related to the reservoir performance significantly (Bodvarsson et al., 1980). More information is needed regarding the two phase flow of water and steam in porous medium and the application of relative permeabilities. The purpose of this study was to address this need by performing an experiment where two phase mixture of a geothermal fluid was injected into relatively large tube filled with porous material. The relative permeabilities were calculated from the directly measured parameters. The dimensions of the tube were selected to reduce the end and wall effects of the device. The conditions may therefore to some extent resemble a geothermal reservoir better than those in many of the previous experiments.

3.3.2 Experimental procedure

A process diagram of the measurement device used for the experiments is shown in Fig. 3.15 and the components are described in the equipment list in Table 3.2. The main component was an insulated steel pipe (component E in Table 3.2 and Fig. 3.15) filled with porous material. It had flanges on each end, enabling change of filling material. The pipe was supported on a bracket enabling rotation so the

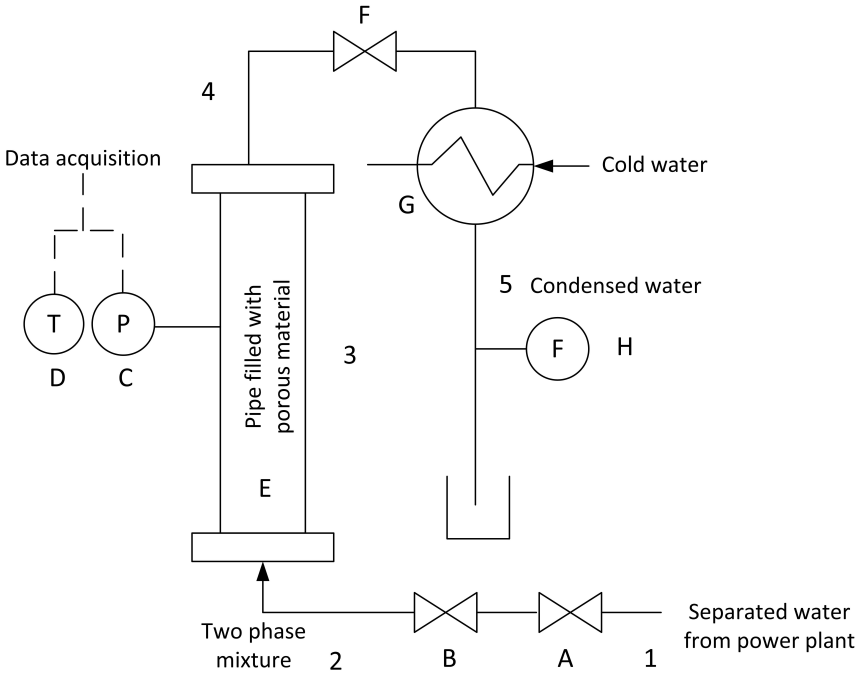

Figure 3.15: A process diagram showing the main components and fluid states in the measurement device designed and constructed for this study. The components are described in Table 3.2.

flow direction could be changed. Fig. 3.16 shows a photo and a 3D drawing of the experimental device.

The fluid used for the experiments was of geothermal origin flowing from separators at Reykjanes geothermal power plant (HSOrka, 2015). The reservoir fluid at the Reykjanes geothermal field is hydrothermally altered seawater with magmatic gases and high in salinity (Arnorsson, 1978) (Fridriksson et al., 2010). The seawater near the coast of Reykjanes has chloride (Cl) concentration of 19100 mg/kg and the Reykjanes wells have Cl concentration ranging from 18000-21000 mg/kg (Fridriksson et al., 2010) or 3.2 wt% NaCl (Hardardottir et al., 2010). The average silica (SiO_2) concentration in the Reykjanes wells is 665 mg/kg (Hardardottir et al., 2010). The fluid used for the experiments flowed from the steam separator in the power plant as saturated water at 210°C and 19 bar_a. The turbines in the power plant are operated at this inlet pressure which is unusually high compared to other geothermal power plants (Yamaguchi, 2010). The reason for the high separation pressure is to prevent silica scaling. For lower separation pressures it is more likely that serious silica scaling issues arise. The reservoir fluid temperature is up to 315-320°C (Freedman et al., 2009) (Hardardottir et al., 2009) which according to the amorphous silica (Fournier and Rowe, 1977) and quartz (Fournier and Potter, 1982) solubility curves will result in silica scaling occurring at separation temperatures even above 200°C.

Table 3.2: Description of the components of the measurement device. Letters refer to Fig. 3.15.

Component	Component name	Description
A	Stop valve	D=1 inch
B	Throttle valve	D=1 inch
C	Pressure sensor and indicator	Tecsis 4-20mA (Tecsis, 2015) and indicator
D	Temperature sensor	Thermocouple
E	Pipe filled with porous material	D=10 inch, t=5mm, L=4 m
F	Back pressure valve	D=1 inch
G	Condenser/cooler	Heat exchanger
H	Flow meter	Mass and time measurement

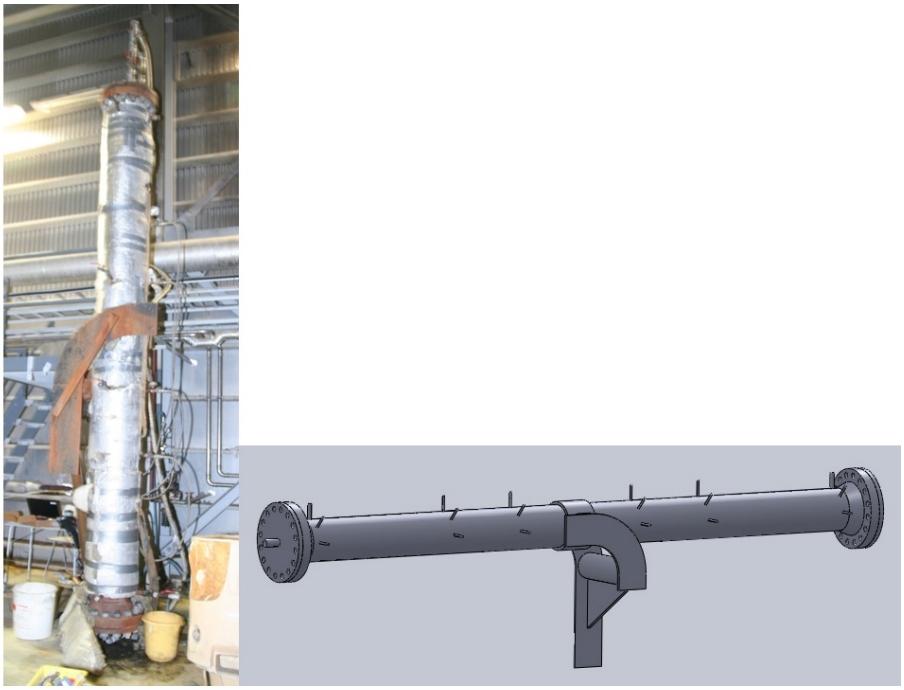

Figure 3.16: A photo showing the experimental setup and a 3D drawing showing the pipe on the steel bracket.

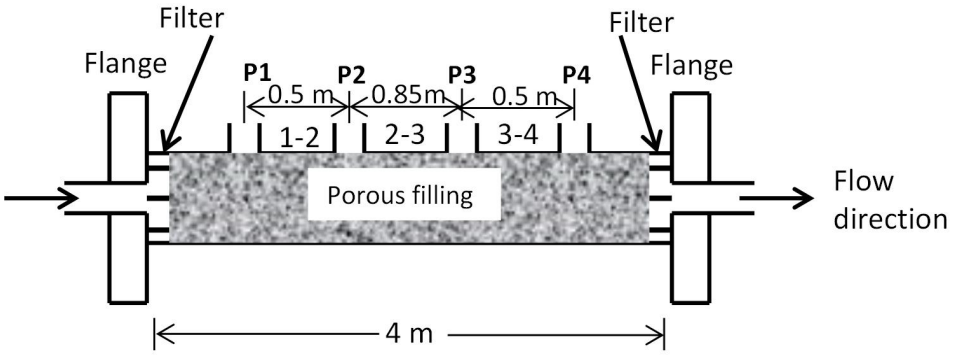

Figure 3.17: Location of pressure sensors on the measurement device.

The effect of salinity however results in higher silica solubility (Von Damm et al., 1991) but same temperature limits for silica prevention are expected.

The separated fluid was used to produce a two phase mixture in a throttle valve (component B) in Fig. 3.15 by lowering the pressure and thereby causing flashing. The fluid used for the experiments flowed through an approximately 20 m long pipeline from the separator to the device. Even though the pipeline was well insulated a considerable heat loss occurred on the way. The enthalpy at the device inlet (state 2 in Fig. 3.15) was measured with a tracer analysis method described by Lovelock (2001) and was 855 kJ/kg. The enthalpy therefore decreased from 890 kJ/kg, which was the saturation condition in the separator, due to heat loss in the pipeline.

After a two phase mixture was formed in the throttle valve (component B) it was injected into the pipe (component E). As the two phase mixture flowed through the resistive filling its pressure decreased. The fluid pressure was measured and logged at four locations on the pipe, see Fig. 3.17. As the pressure was logged continuously it could be observed when steady state condition of the flow was reached.

At the exit of the pipe (state 4 on Fig. 3.15) a valve (component F) was installed to control the back pressure. The condenser (component G) condensed the two phase mixture exiting the device and a manual flow measurement (component H) was made for the condensed water to determine the total mass flow, $\dot{m}_t$ through the pipe. The condenser consisted of a small diameter pipe, which the two phase mixture was flowing through, immersed in a cold water tank. To determine the mass flow of each phase Eqs. (2.15) and (2.16) were used and the steam fraction x was calculated using Eq. (2.17) where the saturation enthalpies for water and steam were calculated from the measured pressure values P1 to P4 in Fig. 3.17 and h_t was the measured total enthalpy of the fluid.

The intrinsic permeability, k, of the porous filling inside the pipe had to be de-

Table 3.3: List of setups for the measurements, the vertical flows were upwards against gravity.

Setup	Filling type	Direction
1. Sand	Crushed basalt 0 - 2 mm grain size	Vertical
2. Sand	Crushed basalt 0 - 2 mm grain size	Horizontal
3. Sand and gravel	Crushed basalt 0 - 5 mm grain size	Vertical
4. Sand and gravel	Crushed basalt 0 - 5 mm grain size	Horizontal

termined for the relative permeability calculations in Eqs (2.6) and (2.7). It was measured using single phase water from the condenser outlet in the power plant at 40° C and 19 bar_a. The intrinsic permeability was determined using Eq. (2.1).

With the collected data, that is the pressure at locations P1 to P4 in Fig. 3.17, the total mass flow measurement, the measured intrinsic permeability and phase mass flow determinations from Eqs (2.15) and (2.16), the relative permeabilities could be calculated using Eqs (2.6) and (2.7) as shown in Eqs (3.19) and (3.20) where the body forces $\rho_w g$ and $\rho_s g$ applied only to the vertical flow cases where the flow was upwards against gravity.

$$k_{rw} = -\frac{\frac{\dot{m}_w}{A}\nu_w}{k(\frac{\Delta p}{\Delta x} + \rho_w g)} \tag{3.19}$$

$$k_{rs} = -\frac{\frac{\dot{m}_s}{A}\nu_s}{k(\frac{\Delta p}{\Delta x} + \rho_s g)} \tag{3.20}$$

where $\Delta p/\Delta x$ is the measured pressure gradient of the two phase flow and A is the area of the flow channel.

After the measurement device was initially run with condensed water to determine the intrinsic permeability, it was run with a two phase mixture using four different setups, listed in Table 3.3. Measurements for each setup were conducted multiple times with different inlet pressure and mass flow. The intrinsic permeability was measured between the runs to see if it had changed during the two phase runs.

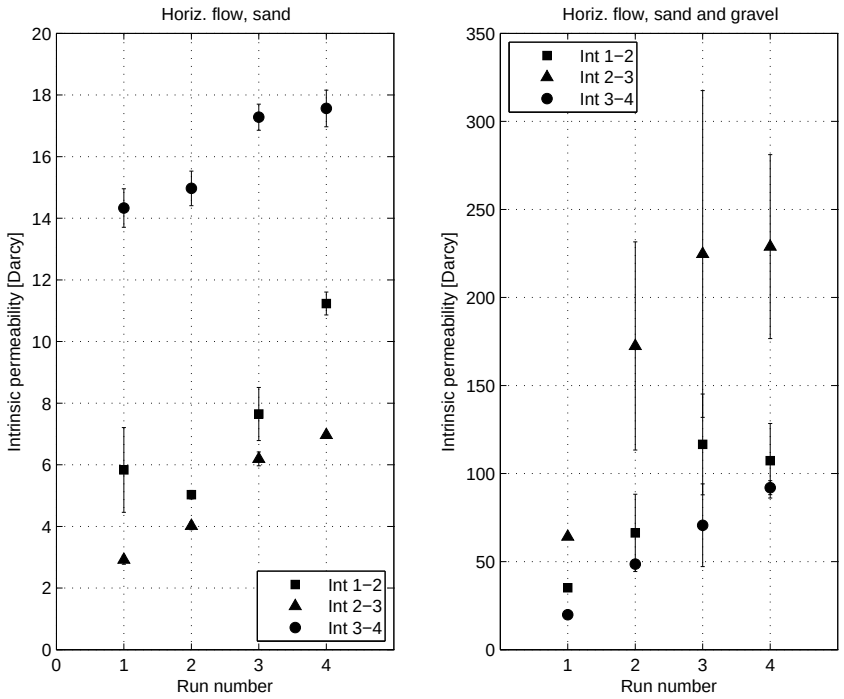

Figure 3.18: Result of measurements of the intrinsic permeabilities for sand (left) and sand-gravel (right) filled column, for horizontal flow direction. Number of runs correlated with increasing time.

3.3.3 Summary of results and discussion

Intrinsic Permeability Measurements

Before being able to calculate the relative permeabilities, the intrinsic permeability was calculated from the measured values of water phase only. The results are shown in Figs 3.18 and 3.19. The intervals defined in Figs 3.18 and 3.19 are related to pressure ports P1-P2 (Int 1-2), P2-P3 (Int 2-3) and P3-P4 (Int 3-4) seen in Fig. 3.17 where the results are shown for the four experiments setups listed in Table 3.3. The plots show the mean value of the intrinsic permeabilities and the error bars are two standard deviations in total.

Relative Permeability Measurements

The intrinsic permeabilities were then used to calculate the relative permeabilities, taking into account the variance in the intrinsic permeability. The relative permeabilities for the two phase flow were calculated according to the methods described

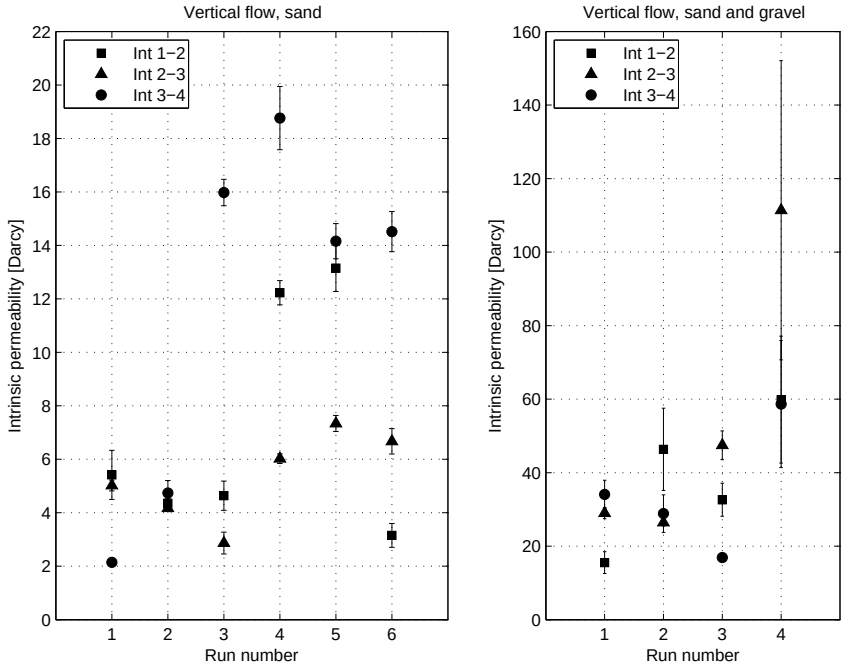

Figure 3.19: Result of measurements of the intrinsic permeabilities for sand (left) and sand-gravel (right) filled column, for vertical flow direction. Number of runs correlated with increasing time.

in Section 3.3.2 by using the direct measured values and Eqs (3.19) and (3.20). The results obtained by using Eq. (2.13) were also considered but did not lead to considerable differences. It should be noted, that the water saturation could not be measured directly in this experiment and plots of the relative permeabilities similar to Fig. 2.1 could therefore not be made. For comparison purposes the two relative permeabilities were plotted in Fig. 3.20 for the setups listed in Table 3.3 together with the X Curve, the Corey curve (Corey, 1954) and the Functions of Verma (Verma, 1986).

Although the local water saturation was not known, the flowing saturation defined in Eq. (2.20) could be determined. The relative permeabilities were plotted as functions of the flowing saturations as shown in Fig. 3.21 for the setups listed in Table 3.3.

By using the relation shown in Eq. (2.21) connecting the flowing saturation $S_{w,f}$ and the local water saturation S_w, the local water saturation could be estimated and the relative permeabilities compared to relative permeability curves as seen in Fig. 3.22. Fig. 3.23 shows the cases where the pipe was filled with sand only.

The results in Fig. 3.20 show that the relative permeabilities deviate from the X-curves, therefore supporting the idea that they are not linearly dependant on water

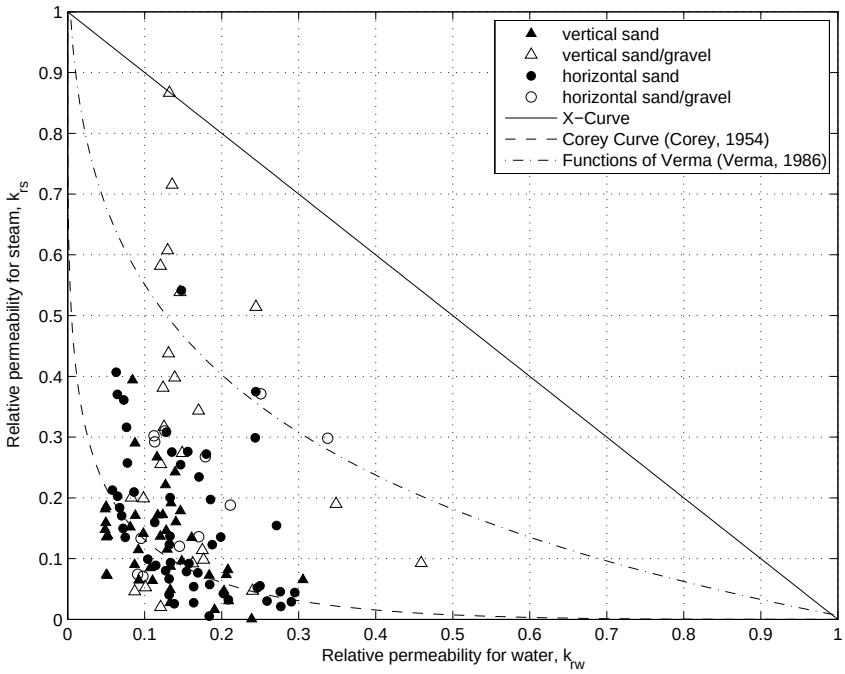

Figure 3.20: Calculated relative permeabilities from the experimental measurements, compared with curves found in literature.

saturation. The results also show, that for many of the values, the calculated relative permeabilities are located between the Corey curves and the Functions of Verma. That indicates that the phase interaction is smaller than proposed by the Corey curves but higher than proposed by the Functions of Verma.

The relative permeabilities form a scattered cloud instead of a clear line such as a relative permeability curves do. One of the main factors contributing to the errors in the experimental procedure is the determination of the intrinsic permeabilities as seen in Figs 3.18 and 3.19 which show a large variance in the intrinsic permeabilities. That might result from the different packing distribution or scaling occurring mainly at specific locations in the pipe. The variance in the intrinsic permeabilities may also be due to the fact that some of the smaller particles in the filling were washed out through the filter holding the porous material in place, thereby increasing the intrinsic permeability between runs. When the brine was flashed through the pipe its pressure and correspondingly the temperature decreased to values below the temperature limit for silica scaling to occur. When the pipe was emptied silica scaling could be observed within the porous material that the pipe was filled with. This nature of silica precipitation in porous material is known in geothermal applications. Silica precipitation rate in porous materials has been reported in order to predict the effect of it for reinjection sites. In a study by Mroczek et al. (2000) the silica deposition rates were measured experimentally and the results used for predicting the effect of injecting brine into the reservoir at Wairakei. The results predicted

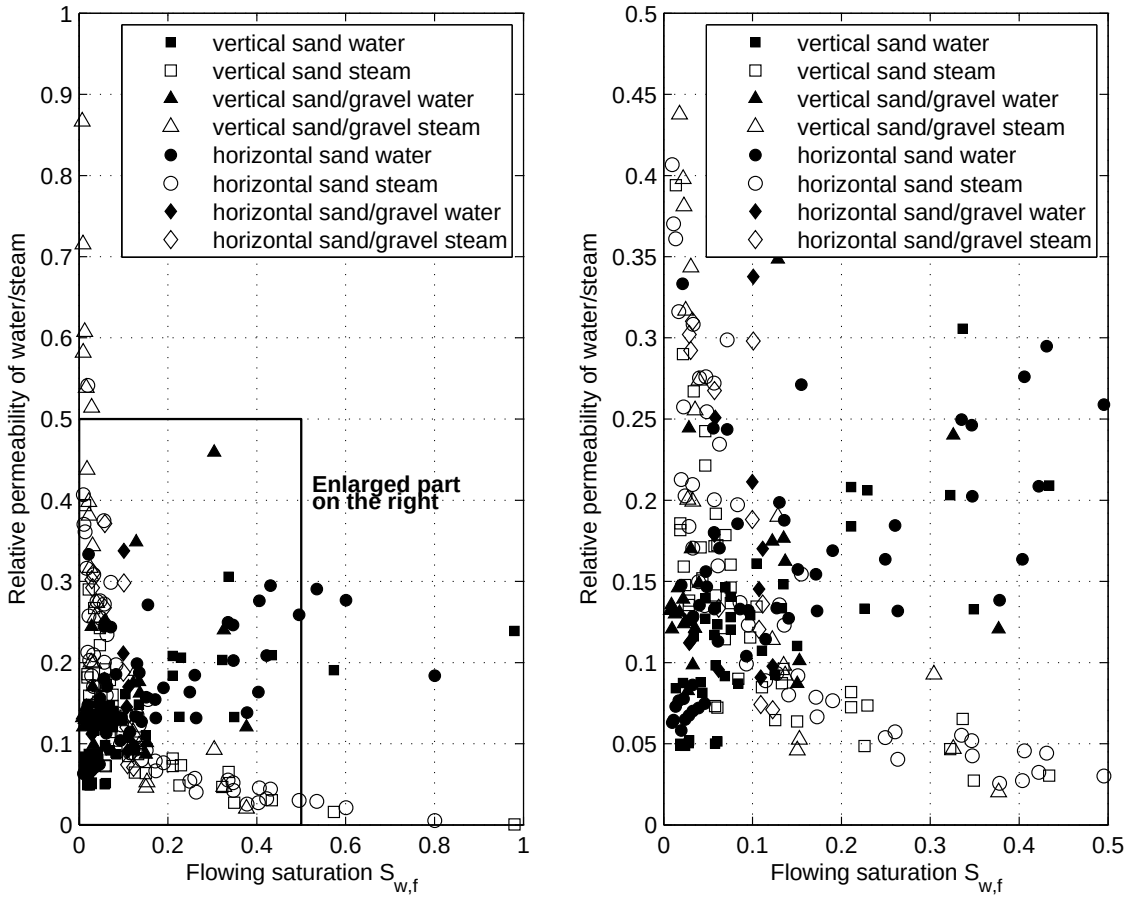

Figure 3.21: The relative permeabilities from Fig. 3.20 as functions of the flowing saturations, the graph on the right side is an enlarged part of the graph on the left side.

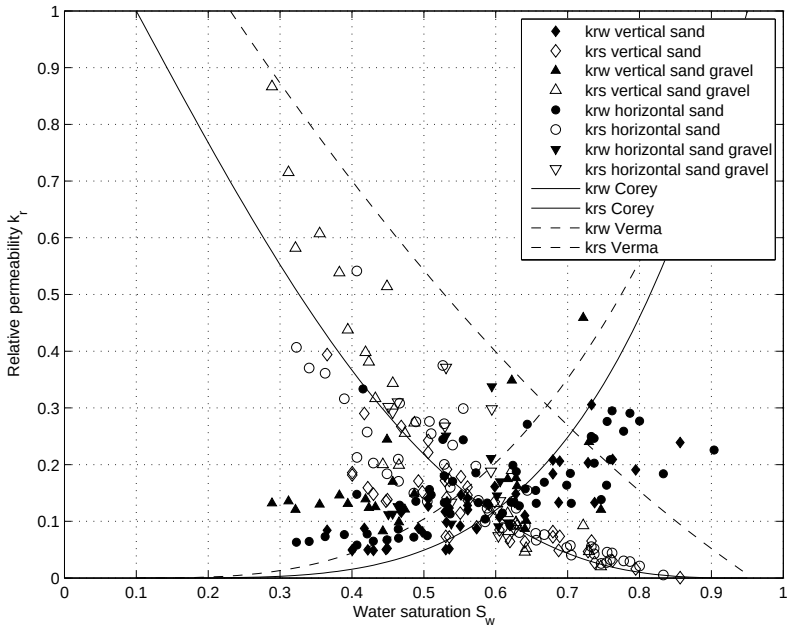

Figure 3.22: The calculated relative permeabilities as functions of the local saturation, gained from Eq. (2.21) for all four flow cases listed in Table 3.3. For the Corey and the Verma Curves $S_{wr} = 0.1$ and $S_{sr} = 0.05$.

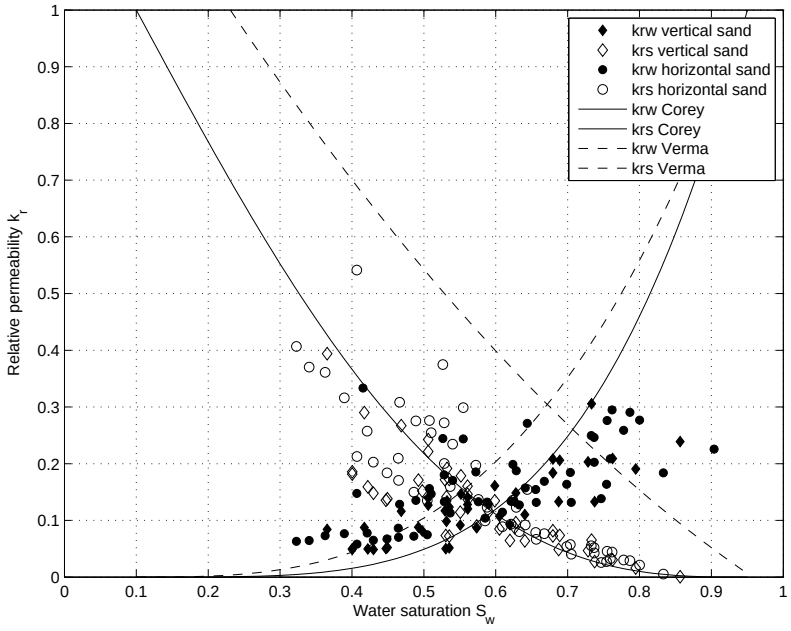

Figure 3.23: The calculated relative permeabilities as functions of the local saturation for the cases shown in Fig. 3.22 where the device was filled with sand.

a permeability reduction in the vicinity of the well. This behaviour was detected for vertical flow through the smaller grain size. For larger grain size other factors changing the intrinsic permeability, like the nonuniform packing, seem to have had a larger effect.

The data points for setups 3 and 4 (see Table 3.3) where filling material with larger grain size was used, shows high variance in the relative permeabilities as seen in 3.23. The stability of the intrinsic permeability was also low for that filling type as seen in Figs 3.18 and 3.19 which results in higher error factors in the calculation of relative permeabilities for that setup. Fig. 3.23 can therefore be compared to Fig. 3.22 showing less variance of the relative permeabilities when only results using sand are shown.

In spite of those error factors, the measurements show a resemblance to a real geothermal reservoir since the geothermal fluid normally does not flow at controlled conditions in the reservoir. Factors like precipitation of minerals and varying intrinsic permeability are likely to be observed in real cases. In Fig. 3.21 the relative permeabilities follow a pattern where water relative permeabilities increase with the flowing saturation $S_{w,f}$ and the relative permeabilities of steam decreases with increasing $S_{w,f}$. When the local water saturation was determined using Eq. (2.21) the relative permeabilities shown in Fig. 3.22 shift in the saturation range from Fig. 3.21 indicating that the flowing saturation is underestimated. That was also the result in a study found in literature (Reyes et al., 2004).

As seen in Fig. 3.20 no clear difference is seen between the relative permeabilities if the flow direction is horizontal or vertical. That does not necessarily mean that the flow direction is not affecting them. In this setup the pressure gradient was significantly higher than the body force due to gravity, leading to only small effects of the gravity on the overall measurements according to Eqs (2.6) and (2.7).

In Fig. 3.20 it can be observed, that the relative permeabilities of water appear to be almost constant for higher values of the steam fraction x. The reason can be that with increasing steam content, the velocity increases due to lower density of the mixture. The fluid might push the grains of which the filling consists of to the side, leading to higher intrinsic permeabilities which is then not accounted for when calculating the relative permeabilities. Using higher values of the intrinsic permeabilities for these points (where the water saturation is low) would result in lower relative permeabilities.

In Fig. 3.22 the steam relative permeabilities follow the Corey curve quite well, but the water relative permeabilities do not. For lower water saturations the error in intrinsic permeabilities measurements might have resulted in larger relative permeabilities of water due to the reasons as already stated. For larger water saturations the relative permeabilities of water are however lower than the Corey curves. This

indicates that there is more interaction among these values than predicted by the Corey curves.

3.3.4 Conclusions of Paper III

In this study, geothermal fluid was used to calculate the relative permeabilities for water and steam in porous material. The resulting relative permeabilities follow the Corey curves to some extent, but due to variance in the intrinsic permeabilities the relative permeabilities are scattered. In geothermal reservoirs, the intrinsic permeabilities can hardly be considered constant so the results here give a valuable information for the application of relative permeabilities in geothermal reservoirs.

3.4 Paper IV

Calculations of relative permeabilities from field data and comparison to laboratory measurements

3.4.1 Introduction

This study refers to the research described in Gudjonsdottir et al. (2015a) which is appended to this thesis. A method introduced by Shinohara (1978) was presented in Section 2.3. This method was applied to data from three Icelandic geothermal fields; Reykjanes, Nesjavellir and Hellisheidi. Available data on well discharge and enthalpy were used to calculate the relative permeabilities for the downhole two phase reservoir flow for each well used in the study. The enthalpy measurements were available from flow tests using tracers (Hirtz et al., 2001) (Lovelock, 2001) and Russell James method (James, 1962). The mass flow and enthalpy were known from the wellhead condition and downhole temperature was determined from temperature profiles from the wells. It is important for this method to use as accurate temperature values as available for the reservoir fluid since the relative permeabilities depend on the viscosities (see Eqs (2.11) and (2.12)) which are highly temperature dependant.

3.4.2 Field data

Reykjanes geothermal area

The Reykjanes geothermal area has been utilized for power production since 2005 and has 2x50 MW condensing turbines operating (Ragnarsson, 2015), (Bertani, 2012). A map of the area is shown in Fig. 3.24. The wells that were used for these calculations were wells RN11, RN12, RN14, RN18, RN19, RN21, RN22, RN23, RN24 and RN27. Enthalpy and mass flow measurements used for this study are from years 2010-2012 where several enthalpy measurements were available for each well.

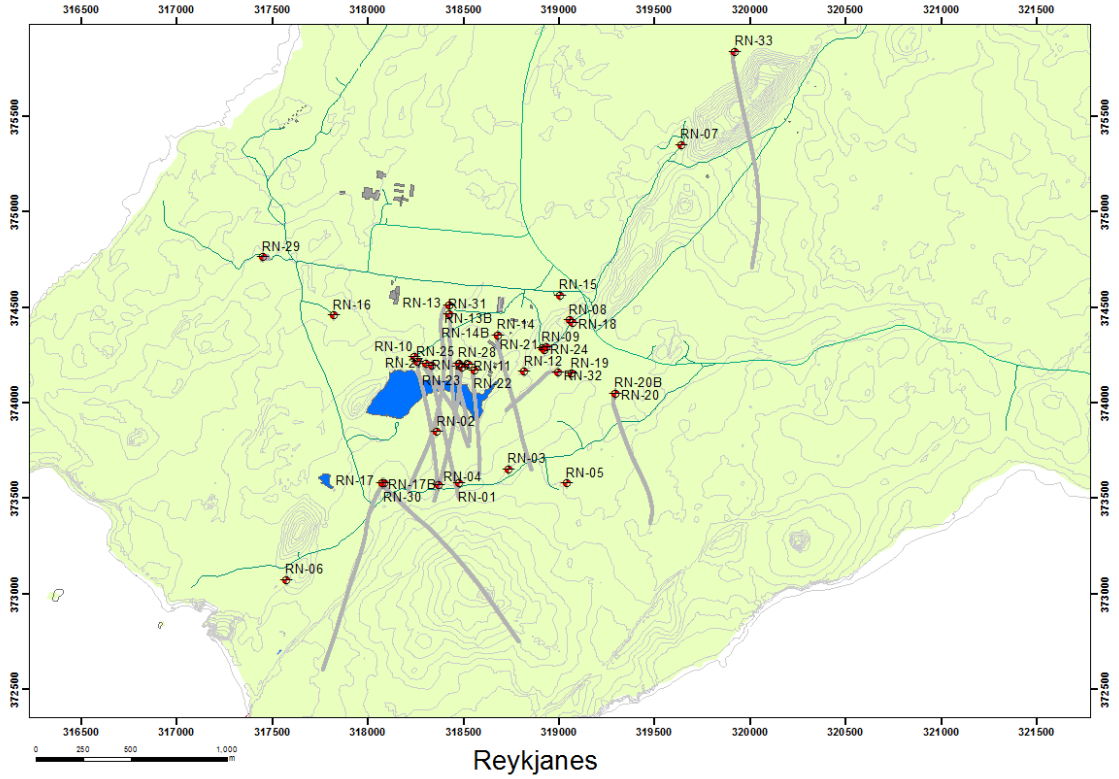

Figure 3.24: A map of the Reykjanes geothermal field and the location of geothermal wells. Courtesy of HS Orka and ISOR.

Hellisheidi geothermal area

The Hellisheidi geothermal area has been utilized for power production since 2006 and has 6x45 MW condensing turbines plus 1x33 MW low pressure condensing tur-

bine operating (Ragnarsson, 2015), (Bertani, 2012) as well as capacity of producing 133 MW of thermal energy (ReykjavikEnergy, 2015). A map of the area is shown in Fig. 3.25. The wells that were used for these calculations were wells HE06, HE07, HE09, HE12, HE15, HE17, HE18, HE19, HE29, HE30, HE47 and HE50. Enthalpy and mass flow measurements used for this study are from years 2008-2013 where several enthalpy measurements were available for each well.

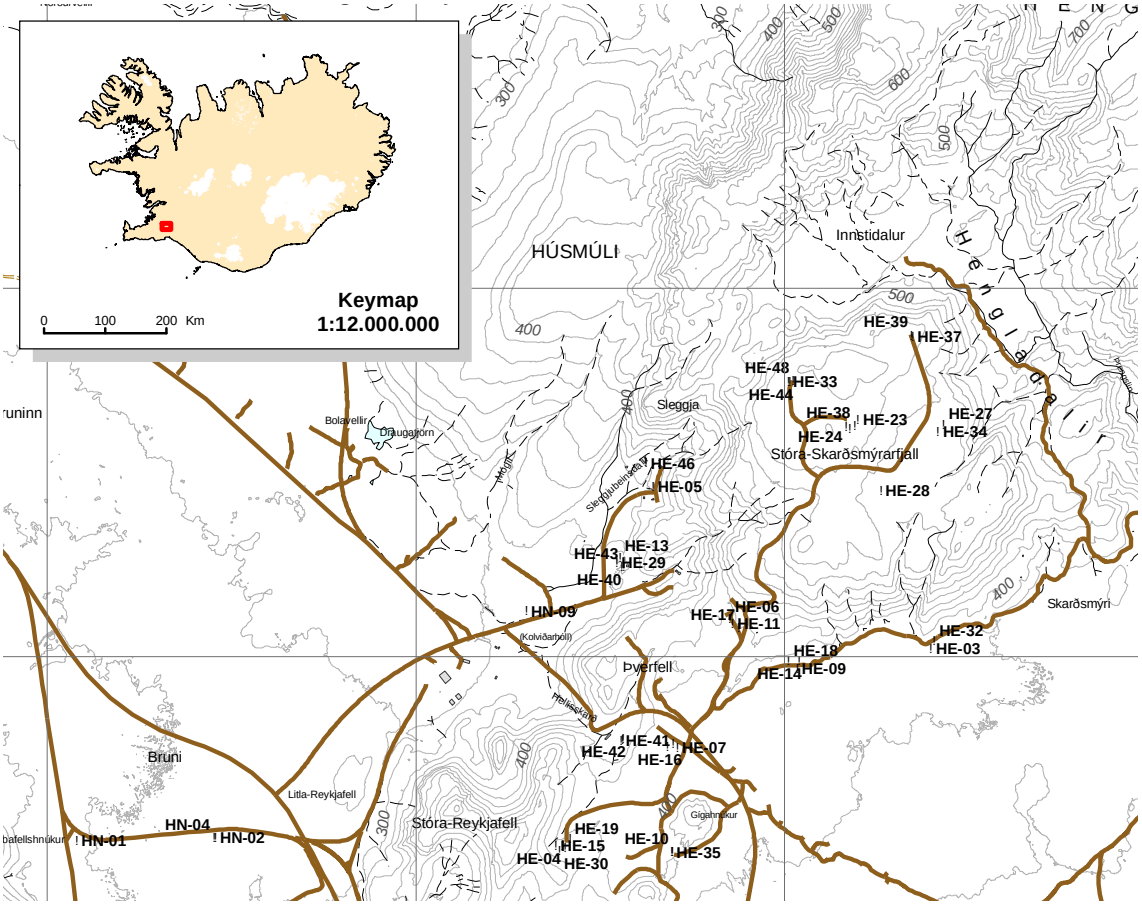

Figure 3.25: A map of the Hellisheidi geothermal field and the location of geothermal wells. Courtesy of Reykjavik Energy and ISOR.

Nesjavellir geothermal area

The Nesjavellir geothermal area has been utilized for power production since 1998 and has 4x30 MW condensing turbines operating as well as capacity of producing 300 MW of thermal energy (Ragnarsson, 2015), (Bertani, 2012). A map showing the area is shown in Fig. 3.26. The wells that were used for these calculations were wells NG06, NG10, NJ11, NJ13, NJ16, NJ21, NJ22 and NJ24. Enthalpy and mass flow

measurements used for this study are from years 2000-2013 where several enthalpy measurements were available for each well.

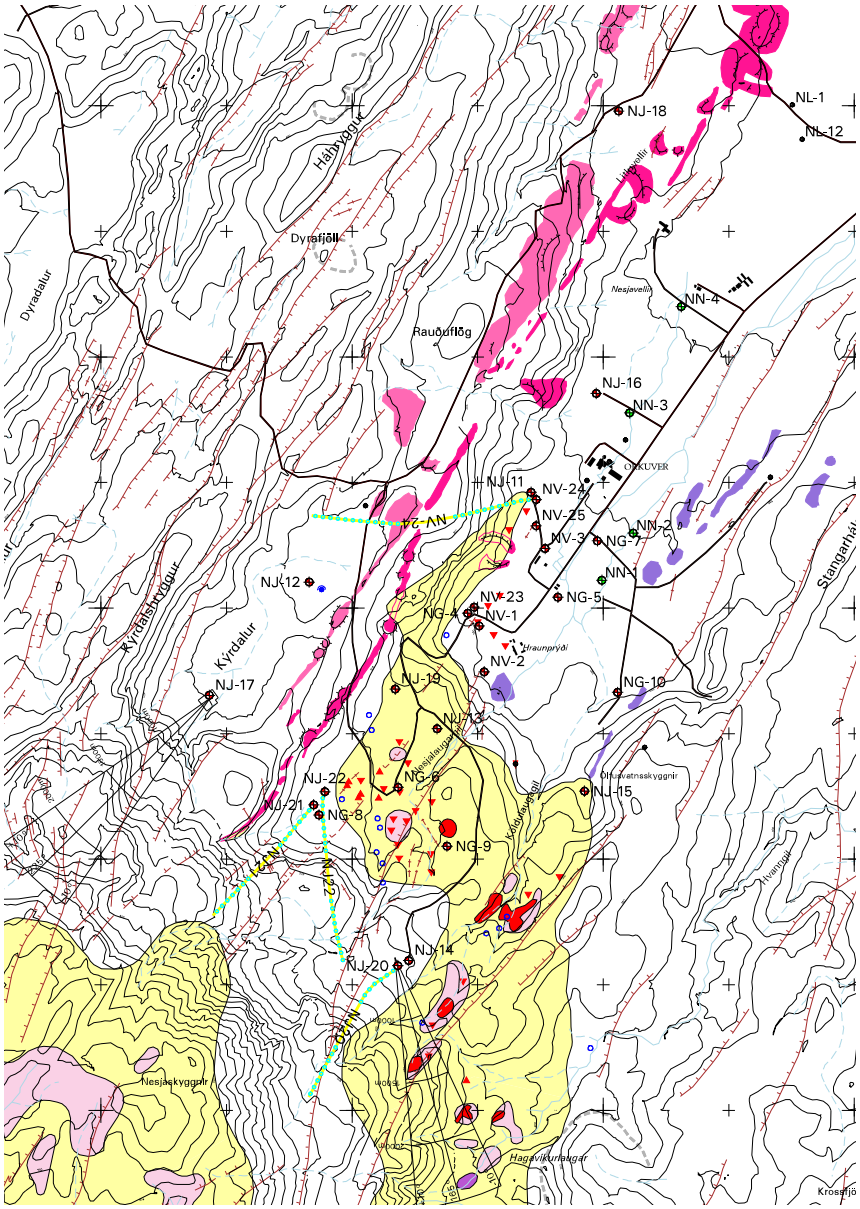

Figure 3.26: A map of the Nesjavellir geothermal field and the location of geothermal wells. Courtesy of Reykjavik Energy and ISOR.

The results from the relative permeability calculations from field data were compared to measured values from laboratory experiments which were described in Chapter 3.3.

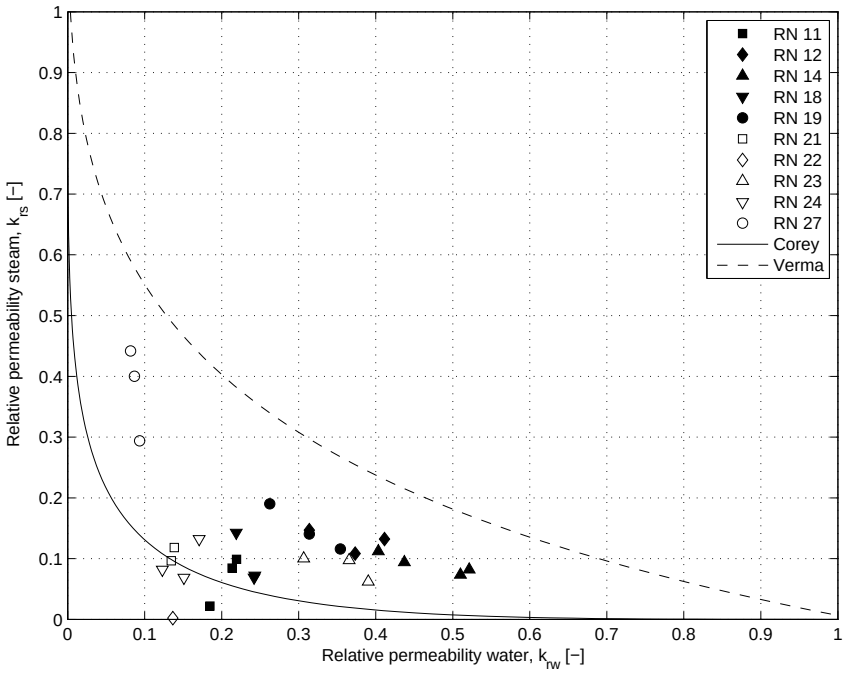

Figure 3.27: Relative permeabilities from Reykjanes wells calculated with the Shinohara method as well as the Corey curve (Corey, 1954) and Functions of Verma (Verma, 1986).

3.4.3 Summary of results and discussion

Figs. 3.27 to 3.29 show the results of relative permeability calculations for the wells at the three geothermal fields in Iceland that the Shinohara method was used on. Fig. 3.30 shows the results of the field relative permeabilities as calculated using the Shinohara method together with the calculated relative permeabilities from measurements shown in Fig. 3.22.

The flowing water saturation was calculated according to Eq. (2.20) and the actual water saturation was then calculated according to Eq. (2.21). They vs. the relative permeabilities are shown in Figs 3.31 and 3.32.

Although the relative permeability values shown in Fig. 3.32 are scattered and they do not follow any clear relative permeability curve, it is clear that the relative permeabilities show curvilinear behaviour to the water saturation. This applies both for the laboratory data as well as the field data. According to Fig. 3.30 the experimental data follows the Corey curve more closely than the field data does. The reason for this difference can be that the relative permeabilities from the experimental data represent two phase flow in a porous matrix rather than in fractured material as the relative permeabilities from the field data do.

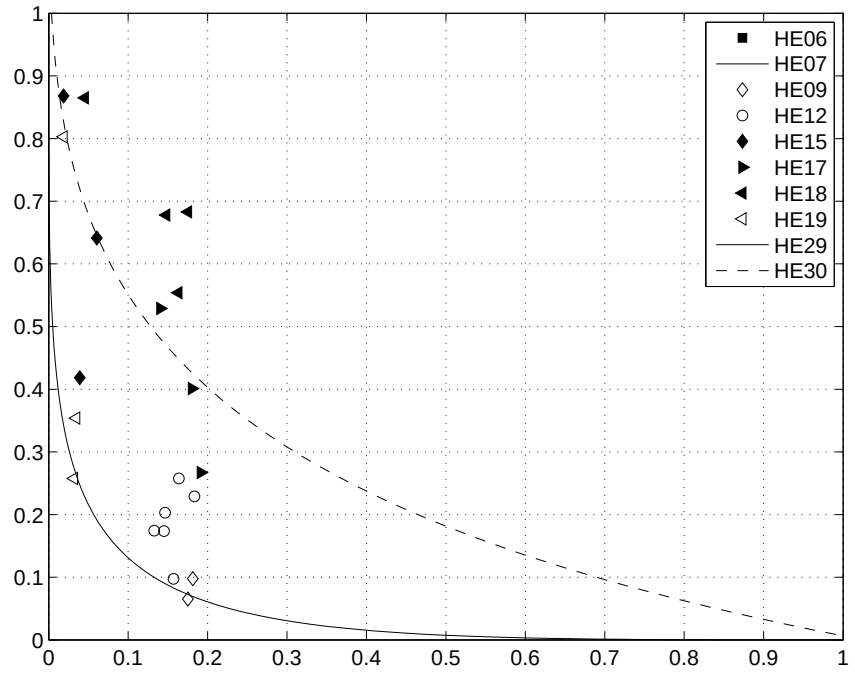

Figure 3.28: Relative permeabilities from Hellisheidi wells calculated with the Shinohara method as well as the Corey curve (Corey, 1954) and Functions of Verma (Verma, 1986).

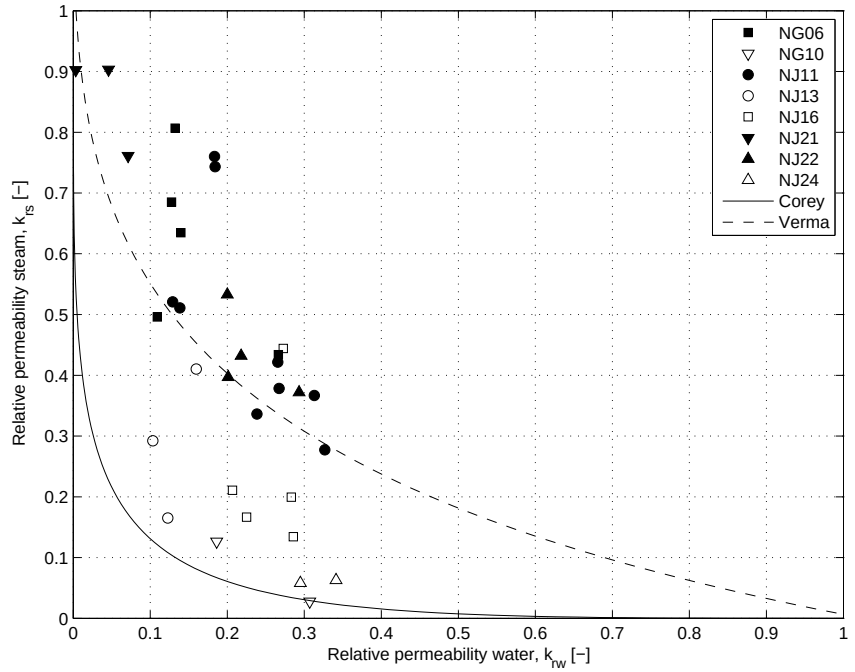

Figure 3.29: Relative permeabilities from Nesjavellir wells calculated with the Shinohara method as well as the Corey curve (Corey, 1954) and Functions of Verma (Verma, 1986).

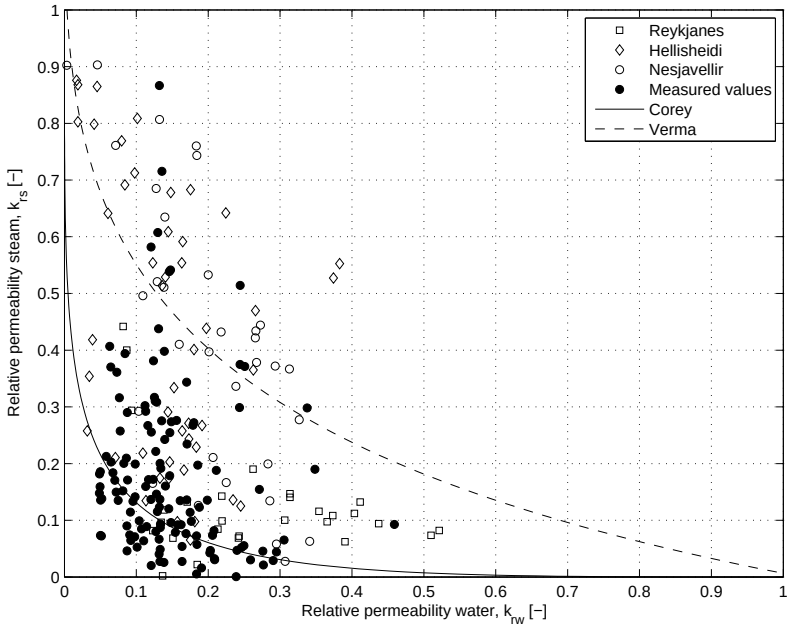

Figure 3.30: Comparison of measured values from laboratory measurements and data from geothermal wells as well as the Corey curve (Corey, 1954) and Functions of Verma (Verma, 1986).

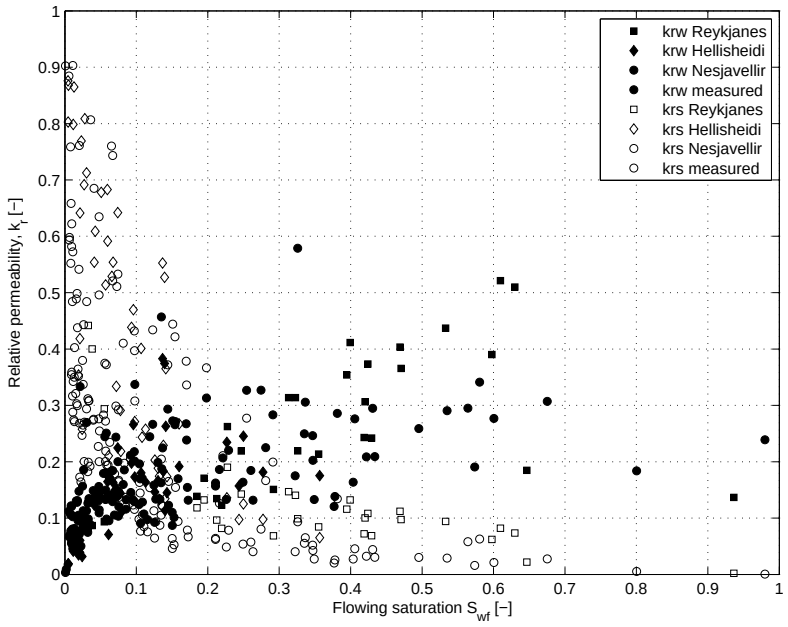

Figure 3.31: The relative permeabilities of measured values from laboratory measurements and data from geothermal wells as functions of the flowing saturation.

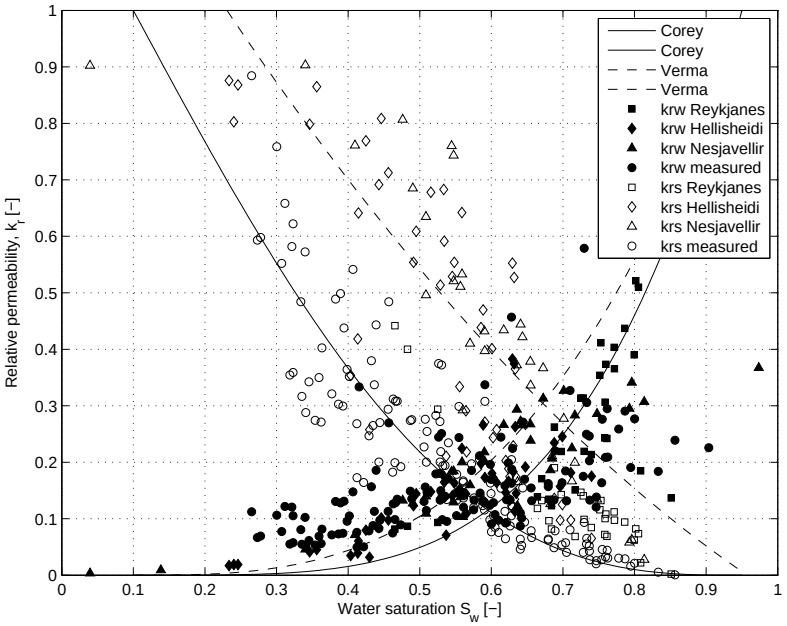

Figure 3.32: The relative permeabilites as functions of the actual water saturation together with the Corey curve (Corey, 1954) and Functions of Verma (Verma, 1986).

The intersection of the steam and the water relative permeabilities occurs for much lower flowing saturations than for the actual (local) water saturation, resulting from the underestimation of the flowing saturation compared to the local water saturation. This can be seen by comparing Fig. 3.31 to Fig. 3.32.

The relative permeabilities from the Reykjanes wells shown in Fig. 3.27 show better correlation to known relative permeability curves than the Hellisheidi and Nesjavellir wells do. Apparently the wells for Hellisheidi and Nesjavellir in Figs 3.28 and 3.29 divide into two groups, one group following the Verma curve to some extent and the other group follows the Corey curve. The data used for the relative permeability calculations using the Shinohara method are measured values at the wellhead which represent a mixture of the fluid flow from different fractures in the reservoir. The well data therefore represents the well average rather than characteristic behaviour of each feedzone. This can account for the fact that wells in the same field can follow different relative permeability curves since each well can produce fluid from different formation than the neighbouring well in the field does.

3.4.4 Conclusions of Paper IV

In this study, the Shinohara method was used to calculate the relative permeabilities for field data for three geothermal areas in Iceland. The resulting relative permeabilities were compared to the values gained from laboratory experiments described in Paper III. The relative permeabilities from the field data indicate less interaction between the two phases than for the laboratory results. This can be explained by the fact that the reservoirs consist of fractured rock rather than porous material as was used in the experiments.

4 Conclusions and future work

The focus in this thesis was on the relative permeability theory and its application on geothermal reservoirs. When modelling two phase flow in geothermal reservoirs, an arbitrary selection of the relative permeability curves has to be made which may or may not resemble the actual interrelation between the water and the steam phase. In reality, the flow will rarely follow one curve and when collecting information from reservoirs, scattering of data points is likely to be seen. Therefore, the path from the concept to reality of the relative permeability is expected to be as seen in Fig. 4.1 where data from this thesis is shown. According to these figures, that results from modelling only, will hardly be exactly the same as real values.

In Fig.4.1a the Corey relative permeability curve is shown. In Fig.4.1b, the results from controlled laboratory measurements are shown together with the Corey curve. In Fig.4.1c the results from large scale laboratory experiments using real geothermal fluid are shown together with the Corey curve. Finally, in Fig.4.1d data from geothermal reservoirs are shown together with the Corey curve.

Geothermal reservoir modelling can give a good prediction about the reservoir's natural behaviour and its response to production. Data from borehole measurements then provides information about the actual response of the reservoir, and those results can be coupled with the reservoir models to make even more detailed models.

In this study, relative permeabilities were calculated using theoretical relations in order to predict whether the flow direction with regard to gravity had an effect on the relative permeabilities. The results show that the direction has an effect which is dependent on the reservoir flow magnitude. These results were supported by water and air measurements, where difference in relative permeabilities with regard to the flow direction was observed. This difference increased with decreasing mass flow. To support this observation, more detailed measurements are needed and using more sophisticated measurement tools could result in more detailed and less scattered results of this effect.

When measurements were performed using a real geothermal fluid in a large scale experiment, variance in the intrinsic permeability values was observed which affected the results. The relative permeability values formed a scattered cloud rather than following a curve. However, since the intrinsic permeability can hardly be considered

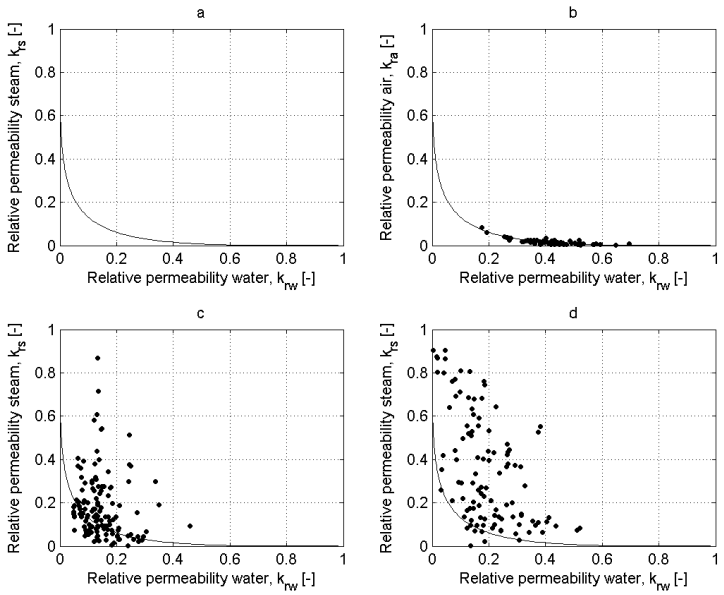

Figure 4.1: Four phases of relative permeability calculations from this thesis together with the Corey curves. a: Corey curve. b: Calculations from water-air measurements. c: Laboratory measurements using real geothermal fluid. d: Calculations from field data.

constant in geothermal reservoirs, these results can be considered to mimic real geothermal reservoirs to a certain extent. The effect of silica scaling on the intrinsic permeabilities in geothermal reservoirs are an important factor, and measurements like this, using real geothermal fluid are an important contribution.

When the Shinohara method was used on data from geothermal reservoirs, the relative permeabilities did not follow known curves explicitly. Using that data resulted in relative permeability values for the reservoir conditions near the wells where the data is collected from. Wells within the same geothermal field were shown to follow different relative permeability curves. That may be due to the fact that the reservoir consists of more than one fracture zone, and each zone has different characteristics and different relative permeability curves may apply for them. This is important to have in mind in geothermal reservoir modelling. It will be interesting to gather future data from these wells to see if the relative permeabilities change with time for the selected wells. Also, this method can be applied to other geothermal fields.

To apply what has been learned from this study into geothermal reservoir models would include the effect of flow direction of the fluid on the relative permeabilities and to estimate the effect of different relative permeability curves within the geothermal reservoirs in general.

Bibliography

Ahmed, N., Sunada, D., 1969. Nonlinear flow in porous media. Journal of the Hydraulics Division, Proceedings of the American Society of Civil Engineers, Vol. 95, no. HY6, Paper 6883, pp. 1847-1857 .

Ambusso, W., 1996. Experimental determination of steam water relative permeability relations. M.Sc. thesis, Stanford University, California .

Arnorsson, S., 1978. Major element chemistry of the geothermal sea-water at Reykjanes and Svartsengi, Iceland. Mineralogical Magazine, Vol. 42, pp. 209-220 .

Arnorsson, S., Stefansson, A., Bjarnason, J., 2007. Fluid-fluid interactions in geothermal systems. Reviews in Mineralogy and Geochemistry, Vol. 65, pp. 259-312 .

Axelsson, G., 2008. Production capacity of geothermal systems. Workshop for Decision Makers on Direct Heating Use of Geothermal Resources in Asia, organized by UNU-GTP, TBLRREM and TBGMED, in Tianjin, China 11-18 May, 2008 .

Axelsson, G., Gunnlaugsson, E., 2000. Long-term monitoring of high- and low-enthalpy fields under exploitation. International Geothermal Association, World Geothermal Congress 2000 Short Course, Kokoneoe, Kyushu District, Japan, May, 226p .

Bertani, R., 2012. Geothermal power generation in the world 2005-2010 update report. Geothermics, Vol. 41, pp. 1-29 .

Bertani, R., 2015. Geothermal power generation in the world 2010-2014 update report. Proceedings World Geothermal Congress 2015, Melbourne Australia, 19-25 April 2015 .

Bodvarsson, G., 1961. Physical characteristics of natural heat sources in Iceland. Proc. UN Conf. on New Sources of Energy, Volume 2. Geothermal Energy, Rome, August 1961. United Nations, New York, pp. 82-89 .

Bodvarsson, G., O'Sullivan, M., Tsang, C., 1980. The sensitivity of geothermal reservoir behavior to relative permeability parameters. Proceedings 6th Workshop on Geothermal Reservoir Engineering, Stanford, 1980, pp. 224-237 .

Brooks, R., Corey, A., 1964. Hydraulic properties of porous media. Hydraulic paper no. 3, Colorado State University .

Brooks, R., Corey, A., 1966. Properties of porous media affecting fluid flow. J. Irrigation and Drainage Division., Proc. ASCE, IR2 (1966), Vol. 92, pp. 61-88 .

Chen, C.Y., 2005. Liquid-gas relative permeabilities in fractures: Effects of flow structures, phase transformation and surface roughness. PhD dissertation, Stanford University, Stanford, California .

Chen, C.Y., Horne, R., 2006. Two-phase flow in rough-walled fractures: Experiments and a flow structure model. Water Resour. Res., Vol. 42, W03430 .

Chen, C.Y., Horne, R., Fourar, M., 2004. Experimental study of liquid-gas flow structure effects on relative permeabilities in a fracture. Water Resour. Res., Vol. 40, W08301 .

Chen, C.Y., Li, K., Horne, R., 2007. Experimental study of phase-transformation effects on relative permeabilities in fractures. October 2007, SPE Reservoir Evaluation & Engineering, pp. 514-526 .

COPRO, 2014. website
http://www.potterseurope.org/documents/files/archive/files/certificates
/ce%20certificate%201137-cpd-0476%20potters%20west%20auckland.pdf
accessed 24.4.2014 .

Corey, A., 1954. The interrelation between gas and oil relative permeabilities. Producers Monthly, Vol. 19, pp. 38-41 .

Darcy, H., 1856. Les fontaines publiques de la ville de Dijon. Dalmont, Paris.

Diomampo, G., 2001. Relative permeability through fractures. M.Sc. thesis, Stanford University, Stanford, California .

DiPippo, R., 2008. Geothermal power plants. Elsevier Ltd.

Fatt, I., Klikoff, W., 1959. Effect of fractional wettability on multiphase flow through porous media. AIME Transactions, pp. 216-246 .

Finsterle, S., Pruess, K., Bullivant, D., O'Sullivan, M., 1997. Application of inverse modeling to geothermal reservoir simulation. Proceedings 22nd Workshop on Geothermal Reservoir Engineering, Stanford University, Stanford, California, pp. 309-316 .

Forchheimer, P., 1901. Wasserbewegung durch boden. Zeitschrift des Vereins Deutscher Ingenieure, No. 45, pp. 1736-1749, pp. 1781-1788 .

Fourar, M., Lenormand, R., 1998. A viscous coupling model for relative permeabilities in fractures. SPE 49006, paper presented at the SPE Annual Technical Conference and Exhibition, New Orleans, LA, USA, pp. 253-258 .

Fournier, R., Potter, R., 1982. A revised and expanded silica (quartz) geothermometer. Geothermal Resource Council Bulletin 11, pp. 3-12 .

Fournier, R., Rowe, J., 1977. The solubility of amorphous silica in water at high temperatures and pressures. American Mineralogy, Vol. 62, pp. 1052-1056 .

Freedman, J., Bird, D., Arnorsson, S., Fridriksson, T., Elders, W., Fridleifsson, G., 2009. Hydrothermal minerals record CO2 partial pressure in the Reykjanes geothermal system, Iceland. American Journal of Science, Vol. 309, pp. 1-46 .

Fridriksson, T., Oladottir, A., Jonsson, P., Eyjolfsdottir, E., 2010. The response of the Reykjanes geothermal system to 100 MWe power production: Fluid chemistry and surface activity. Proceedings World Geothermal Congress 2010, Bali Indonesia, 25-29 April 2010 .

Grant, M., 1977. Permeability reduction factors at Wairakei. Paper 77-HT-52, presented at AICHE-ASME, Heat Transfer Conference, Salt Lake City, Utah, August 1977 .

Grant, M., 1983. Review no. 1 Geothermal reservoir modelling. Geothermics, Vol. 12, No. 4, pp. 251-263 .

Grant, M., Bixley, P., 2011. Geothermal reservoir engineering, second edition. Academic Press.

Gudjonsdottir, M., Palsson, H., Eliasson, J., Saevarsdottir, G., 2015a. Calculation of relative permeabilities from field data and comparison to laboratory measurements. Geothermics, Vol. 54, pp. 1-9 .

Gudjonsdottir, M., Palsson, H., Eliasson, J., Saevarsdottir, G., 2015b. Calculation of relative permeabilities of water and steam from laboratory measurements. Geothermics, Vol. 53, pp. 396-405 .

Hardardottir, V., Brown, K., Fridriksson, T., Hedenquist, J., Hannington, M., Thorhallsson, S., 2009. Metals in deep liquid of the Reykjanes geothermal system, southwest Iceland: Implications for the composition of seafloor black smoker fluids. Geology, Vol. 37, pp. 1103-1106 .

Hardardottir, V., Hedenquist, J., Hannington, M., Brown, K., Fridriksson, T., Thorhallsson, S., 2010. Composition of reservoir liquid and metals in pipeline scale, Reykjanes geothermal system, SW Iceland. Proceedings World Geothermal Congress 2010, Bali Indonesia, 25-29 April 2010 .

Hirtz, P., Kunzman, R., Broaddus, M., Barbitta, J., 2001. Developments in tracer flow testing for geothermal production engineering. Geothermics, Vol. 30, pp. 727-745 .

Horne, R., Satik, C., Mahiya, G., Li, K., Ambusso, W., Tovar, R., Wang, C., Nassori, H., 2000. Steam-water relative permeability. Proceedings World Geothermal Congress 2000, Kyushu-Tohoku, Japan, May 28. - June 10. 2000 .

HSOrka, 2015. website http://www.hsorka.is/english/hsproduction/hsproductionreykjanesvirkjun.aspx accessed 02.10.2015 .

James, R., 1962. Steam-water critical flow through pipes. Proceedings of the Institution of Mechanical Engineers. Vol. 176, No. 1, pp. 741-748 .

Kipp, K., Hsieh, P., Charlton, S., 2008. Guide to the revised ground-water flow and heat transport simulator: HYDROTHERM - version 3. U.S. Geological Survey, Reston, Virginia .

Li, K., 2008. A new method for calculating two-phase relative permeability from resistivity data in porous media. Transport in Porous Media, Vol.74, pp.201-33 .

Li, K., 2010. Correlation between resistivity index, capillary pressure and relative permeability. Proceedings World Geothermal Congress, Bali Indonesia, 25-29 April 2010 .

Li, K., Horne, R., 2002. Calculation of steam-water relative permeability using capillary pressure data. 27th Workshop on geothermal reservoir engineering, Stanford University, Stanford, California .

Li, K., Horne, R., 2004. Steam-water and air-water capillary pressures: Measurement and comparison. Journal of Canadian Petroleum Technology, Vol. 43, pp. 24-30 .

Li, K., Horne, R., 2005a. Inferring relative permeabilities from resistivity well logging. Proceedings 30th Workshop on geothermal reservoir engineering, Stanford University, Stanford, California .

Li, K., Horne, R., 2005b. Steam-water capillary pressure. Proceedings World Geothermal Congress 2005, Antalya, Turkey .

Li, K., Horne, R., 2006. Fractal modeling of capillary pressure curves for The Geysers rocks. Geothermics, Vol. 35, pp. 198-207 .

Li, K., Horne, R., 2007. Systematic study of steam-water capillary pressure. Geothermics, Vol. 36, pp. 558-574 .

Lovelock, B., 2001. Steam flow measurement using alcohol tracers. Geothermics, Vol. 30, pp. 641-654 .

Lund, J., Boyd, T., 2015. Direct utilization of geothermal energy 2015 worldwide review. Proceedings World Geothermal Congress 2015, Melbourne Australia, 19-25 April 2015 .

Mahiya, G., 1999. Experimental measurement of steam-water relative permeability. M.Sc. thesis, Stanford University, Stanford, California .

Mroczek, E., White, S., Graham, D., 2000. Deposition of amophous silica in porous packed beds – predicting the lifetime of reinjection aquifers. Geothermics, Vol. 29, pp. 737-757 .

O'Connor, P., 2001. Constant-pressure measurement of steam-water relative permeability. M.Sc. thesis, Stanford University, Stanford, California .

O'Sullivan, M., Pruess, K., Lippmann, M., 2001. State of the art of geothermal reservoir simulation. Geothermics, Vol. 30, pp. 395-429 .

Piquemal, J., 1994. Saturated steam relative permeabilities of unconsolidated porous media. Transport in Porous Media, Vol. 17, pp. 105-120 .

Pruess, K., Oldenburg, C., Moridis, G., 1999. TOUGH2 user´s guide, version 2.0. Earth Sciences Division, Lawrence Berkeley National Laboratory, University of California, Berkeley, California .

Pruess, K., Tsang, Y., 1990. On two-phase relative permeability and capillary pressure of rough-walled rock fractures. Water Resources Research, Vol. 26, No. 9, pp. 1915-1926 .

Ragnarsson, A., 2015. Geothermal development in Iceland 2010-2014. Proceedings World Geothermal Congress 2015, Melbourne, Australia, 19-25 April 2015 .

Reyes, J., Chen, C.Y., Li, K., Horne, R., 2004. Calculation of steam and water relative permeabilities using field production data, with laboratory verification, in: GRC Transactions, Vol. 28, pp. 609-615.

ReykjavikEnergy, 2015. Website http://www.or.is/en/projects/hellisheidi-geothermal-plant, accessed 11.8.2015 .

Romm, E., 1966. Fluid flow in fractured rocks (Translated from Russian). Nedra Publishing House, [English translation, Blake, W.R., Bartlesville, OK, 1972] .

Sanchez, J., Schechter, R., 1990. Steady adiabatic, two-phase flow of steam and water through porous media. SPE Reservoir Engineering, August 1990, pp. 293-300 .

Sanchez, J., Schechter, R., Monsalve, A., 1986. The effect of trace quantities of surfactant on nitrogen/water relative permeabilities. Paper SPE 15446 presented at the 1986 SPE Annual Technical Conference and Exhibition, New Orleans, Oct. 5-8 .

Sanyal, S., 2005. Classification of geothermal systems - A possible schemes. Proceedings 34th Workshop on Geothermal Reservoir Engineering, Stanford University, Stanford, California, January 31-Feb. 2 2005 .

Satik, C., 1998. A measurement of steam-water relative permeability. Proceedings 23rd Workshop on Geothermal Reservoir Engineering, Stanford University, Stanford, California, pp. 120-126 .

Scheidegger, A., 1974. The physics of flow through porous media, third ed. University of Toronto, Toronto, Canada.

Shinohara, K., 1978. Calculation and use of steam/water relative permeabilities in geothermal reservoirs. M.Sc. thesis, Stanford University, Stanford, California .

Sorey, M., Grant, M., Bradford, E., 1980. Nonlinear effects in two-phase flow to wells in geothermal reservoirs. Water Resources Research, Vol. 26, No. 4, pp. 767-777 .

Speyer, N., 2007. Experimental measurement of two-phase relative permeabilities in synthetic vertical fractures. M.Sc. thesis, Stanford University, California .

Tecsis, 2015. website
http://www.oem.co.uk/products/pressure_flow/pressure_transducers/general_purpose_pressure_transducer/tecsis_-_general_purpose_pressure_transducer/1159157-308251.html
accessed 26.10.2015 .

Todd, D., Mays, L., 2005. Groundwater hydrology, Third Edition. John Wiley and Sons, Inc.

Verma, A., 1986. Effects of phase transformation of steam-water relative permeabilities. Ph.D. thesis. University of California, Berkeley.

Von Damm, K., Bischoff, J., Rosenbauer, R., 1991. Quartz solubility in hydrothermal seawater: An experimental study and equation describing quartz solubility for up to 0.5M NaCl solutions. American Journal of Science, Vol. 291, pp. 977-1007 .

Weir, G., 1991. Geometric properties of two phase flow in geothermal reservoirs. Transport in Porous Media, Vol. 6, pp. 501-517 .

Whitaker, S., 1986. Flow in porous media I: A theoretical derivation of Darcy's law. Transport in Porous Media, Vol. 1, pp. 3-25 .

White, D., 1967. Some principles of geyser activity, mainly from Steamboat Springs, Nevada. American Journal of Science, Vol. 265, pp. 641-684 .

Wyckoff, R., Botset, H., 1936. The flow of gas-liquid mixtures through unconsolidated sands. Physics, Vol. 7, pp. 325-345 .

Yamaguchi, N., 2010. Variety of steam turbines in Svartsengi and Reykjanes geothermal power plants. Proceedings World Geothermal Congress 2010, Bali Indonesia, 25-29 April 2010 .

Zeng, Z., Grigg, R., 2006. A criterion for non-Darcy flow in porous media. Transport in Porous Media, Vol. 63, pp. 57-69 .